

PARITY VIOLATION IN INELASTIC SCATTERING
OF POLARIZED ELECTRONS*

Charles Y. Prescott
Stanford Linear Accelerator Center
Stanford University, Stanford, California 94305 U.S.A.

ABSTRACT

Parity non-conservation has been observed in the inelastic scattering of longitudinally polarized electrons from an unpolarized deuterium target at 19.4 and 22.2 GeV. We find an asymmetry $A = (\sigma_R - \sigma_L)/(\sigma_R + \sigma_L) = (-9.5 \pm 1.6) \times 10^{-5} Q^2$, Q^2 in $(\text{GeV}/c)^2$, for values of Q^2 near 1.4. The statistical and systematic errors are each about 9 percent of the measured asymmetry. This result is consistent with predictions from the standard Weinberg-Salam $SU(2) \times U(1)$ model. Using the simple quark-parton model of the nucleon, we obtain $\sin^2 \theta_W = 0.20 \pm 0.03$.

Invited talk Presented at the Sixth Trieste Conference on
Particle Physics, Trieste, Italy, June 26 - 30, 1978.

*Work supported by the Dept. of Energy under Contract EY-76-C-03-0515.

I. INTRODUCTION

The interest in parity non-conservation has been with us since the fifties, when those effects were first demonstrated in weak interaction charged current processes. The emergence of the Weinberg-Salam $SU(2) \times U(1)$ gauge theory of weak and electromagnetic interactions and more recently a wide variety of alternative gauge theories has again raised the issue of parity non-conservation, this time in connection with the weak neutral currents. The measurement of parity violating effects in electromagnetic interactions and in neutrino induced reactions serves to discriminate between the gauge theory models that have come into existence. Several years ago at SLAC, motivated primarily by the implications of the gauge theory ideas, a program was undertaken to develop the necessary experimental tools for investigating parity violating effects in electromagnetic interactions. Inelastic electron scattering, a process thoroughly investigated experimentally and presumably quite well understood phenomenologically, was a natural place to look for parity violation. Parity violation, observed as a helicity dependent term in the cross section, does not arise from electromagnetic processes even in higher order, and thus is a unique signature of non-electromagnetic processes, presumably the weak interactions. To measure helicity dependent effects in the cross section required development of an intense polarized electron source. The performance parameters of such a source and the sensitivity demanded of the experiments were dictated by the smallness of the anticipated parity violating effects. These effects arise from interference between weak and electromagnetic amplitudes, and

are expected from quite general arguments to be in the order of $G_F Q^2 / (2\sqrt{2} \pi \alpha)$ where G_F is the Fermi coupling constant, α is the fine structure constant, and Q^2 is the four-momentum-transfer-squared. For inelastic scattering at SLAC, the expected parity violating effects in the cross section are around $10^{-4} Q^2$, Q^2 in $(\text{GeV}/c)^2$. Gauge theory predictions included the possibility that the effects could be even smaller, or zero. In order to achieve a significant test of gauge theories, the parity violating asymmetry

$$A = (\sigma_R - \sigma_L) / (\sigma_R + \sigma_L) \quad (1)$$

where σ_R (σ_L) is the cross section for $+$ ($-$) helicity of the incident beam, had to be measured to an accuracy of

$$\Delta A \leq 10^{-5} \quad (2)$$

The then-existing techniques used in inelastic scattering experiments did not provide monitoring or control of experimental parameters at the level of sensitivity we required. The experimental program undertaken several years ago had as its objective the development of beam monitoring and counting techniques capable of achieving sensitivity sufficient for these measurements. Before describing these techniques, a discussion must begin with an understanding of the sources of experimental errors.

(a) Statistical errors: The statistical errors on an asymmetry is $\Delta A = 1/\sqrt{N^+ + N^-}$, where N^+ , N^- are the numbers of detected scattered electrons for \pm helicity beams. Thus we needed to detect more than 10^{10} electrons to obtain sufficient statistical accuracy. It is certain that the accuracy of the measurements can be no better than the statistical accuracy. To achieve these large number of detected scattered electrons required a polarized electron source of high intensity and a detector of

large acceptance. The existing spectrometers were too limited in aperture, so a special spectrometer of large acceptance was constructed using magnets out of existing spectrometers.

Data were taken at 120 pulses per second. At this rate only 10^7 pulses per day were obtained. To achieve 10^{10} counts in a 24 hour day required counting at 10^3 counts per pulse (at SLAC, pulses are only 1.5 μ sec long). These counting rates are too high to be handled by conventional electronic logic. In Section II, the technique of flux counting is described, which achieved for us the objective of high counting rate measurements.

(b) Systematic errors: Our systematic errors came in part from imperfect monitoring or control of beam parameters. The measurement of the parity violating asymmetry, Eq. (1), is obtained by a comparison of scattering for a + helicity beam to that for a - helicity beam. To permit a meaningful comparison required that the + helicity and - helicity beams be identical in all other respects. Section IV describes the beam monitoring system we developed to determine the degree to which beam parameters differed. Small changes in position, angle, energy or other parameters which are correlated with the + or - helicity could generate apparent parity violating effects. The beam monitoring system was developed to give us a quantitative measure of such systematic effects.

(c) Drifts: The measured cross section values are subject to changes caused by external or internal influences in the instruments used. However, drifts in gains or calibrations do not affect an asymmetry measurement, Eq. (1), provided the cross sections $\sigma_{R,L}$ can be measured simultaneously. We approach such a condition by providing a source which

can be reversed between beam pulses 8.3 milliseconds apart. Drifts which are slow compared to the beam pulse spacing will be averaged into both $\sigma_{R,L}$ measurements more or less equally.

The polarized electron source, described in Section III, had capability of the electron helicity being reversed between beam pulses. We chose a randomized pattern of helicity. The reason for randomization was to avoid all patterns of a fixed nature, which could lead to difficulties if periodic components in the signals or beam parameters exist. A randomized pattern assures that measurements of σ_R and σ_L are unbiased with respect to all signals periodic in time.

(d) Backgrounds: Background counts can lead to biases or errors in the measured asymmetries. For us the main source of background were photoproduced and electroproduced π^- 's entering the spectrometer acceptances in momentum and angle. Prior to taking data studies were made of background counts in the detectors. The technique of flux counting described in Section II prohibits the use of conventional methods of background discrimination by electronic means. We chose kinematic points where backgrounds are small compared to electron signals. Asymmetries in the background counts were measured and shown to be negligible.

The philosophy of these measurements could be described as having two parts. First, the sources of errors were monitored and controlled to a level that was small compared to the parity violating asymmetries measured. Secondly, the data that were taken offered a number of internal consistency checks that could be made. Section V describes the consistency checks and the data obtained. In Section VI the measured parity violating asymmetries are compared with predictions from gauge theories.

II. FLUX COUNTING

Before discussing the technique of flux counting, a general description of the experiment is useful. Figure 1 shows the various components in a highly schematic form. The two-mile accelerator is collapsed into the small box labelled "LINAC". Electrons could be injected into the linac from either the usual SLAC gun, providing unpolarized electrons from a thermionic cathode, or from the polarized electron source, which has a GaAs crystal cathode. Accelerated electrons passed through a beam transport system after leaving the linac, where the beam parameters were monitored. The most important of these were energy, current, position and angle at the target. A minicomputer (an LSI-11) monitored these parameters, and adjusted beam line magnets to stabilize position and angle of the beam on the target, and adjusted RF phase of two spare klystrons to stabilize beam energy. The beam of electrons passed through a liquid D₂ target, 30 cm in length, of the circulating type which was able to handle the high beam intensities delivered to it. Polarization of the beam was monitored in separate apparatus (Section IV) using spin-dependent effects in polarized electron-polarized electron elastic scattering (Møller scattering). To make these polarization measurements, the liquid D₂ target was (remotely) moved out of the beam.

Inelastic scattering of polarized electrons from unpolarized deuterium was detected at 4° in a spectrometer. This process had been studied earlier at this angle using unpolarized electrons, and a considerable amount of experimental information was available.¹ For the majority of the data the beam energy was 19.4 GeV and the secondary scattered electron energy was 14.5 GeV. The spectrometer consisted of two bending elements

and a quadrupole, constructed from magnets taken from the 8 GeV/c and 20 GeV/c end-station spectrometers. These were arranged downstream and below the target to detect electrons which scattered at 4° down from the target. The angular acceptances were $\Delta\theta = \pm 7.5$ mrad and $\Delta\phi = \pm 16.6$ mrad. Two counters were placed behind the spectrometer to detect the scattered electrons. The first was an atmospheric gaseous N_2 Cerenkov counter (C). The counter was 3.35 meters long with horizontal and vertical apertures of 70 cm each. At the end of the counter, a spherical mirror collected Cerenkov light and focused it onto the photocathode of a photomultiplier tube placed off axis. Electrons passed out of the Cerenkov counter and into a second electron counter consisting of $9X_0$ thick lead glass (TA) with an aperture of 88 cm (horizontal) by 52 cm (vertical). Cerenkov light produced in the lead glass was viewed by an array of 4 photomultipliers.

A six inch thick wall of lead bricks was placed behind the counters to complete the absorption of electron showers. Photoproduced and electroproduced π 's, μ 's and K's will penetrate or develop hadronic cascades in this wall. Behind the wall was located a third counter (consisting also of lead glass) to detect these penetrating particles. The purpose of this third counter was to measure the amount of the background particles, and to monitor the asymmetry associated with them. The π backgrounds were a small part of the electron signal (amounting to approximately $1\frac{1}{2}\%$ in the TA counter), but even small backgrounds could be serious if they showed a large asymmetry. We measured these backgrounds continuously throughout the experiment, and measured the contribution to be negligibly small (less than 1% correction to the final asymmetries, and consistent with zero).

Figure 2 shows the experimental cross section dependence on the spectrometer momentum E' . The momentum acceptance is superimposed. It is intended to be quite broad to enhance the counting rate. One consequence of this design is the finite acceptance at the elastic peak. The contribution to the counting rate from the elastic peak (about 3%) and the $\Delta(1238)$ resonance (about 2%) is not considered serious because the asymmetries from these states are expected to be approximately the same as from inelastic scattering. The measured cross section for π^- 's (μ^- 's and K^- 's are included) is shown on the same scale as e^- 's; the background rates increase as the spectrometer momentum is lowered.

Flux counting is a technique developed for this experiment to permit measurements of inelastically scattered electrons at the high counting rates in this experiment. For the gas Cerenkov counter, electrons which enter its aperture, produce Cerenkov light that was collected by a spherical mirror and focussed onto a photomultiplier photocathode. The anode current is sent to electronic circuitry, where for each beam pulse it is integrated, digitized and read by the computer. This signal (FLUX) is proportional to the flux of electrons through the counter. We generate a quantity proportional to the scattered cross section (averaged over the acceptance) by normalizing to the incident charge, Q , delivered to the target. For each beam pulse i , we form a cross section (units are arbitrary)

$$\sigma_i^{\pm} = \text{FLUX}/Q_i \quad (3)$$

where + and - refer to the beam helicity.

Extensive tests of procedures were performed using unpolarized electrons from the conventional SLAC gun. First it was necessary to

establish linearity of the electronics. Does the system measure the same cross section as the value of Q delivered to the target increases?

Figure 3 shows the measured cross section values, in arbitrary units, for Q from 1/2 to 15×10^{10} electrons per pulse. Linearity of the electronics appeared good to a few tenths of a percent, for this range of current, but only after careful attention to details of electronics and photomultipliers.

Next we established a calibration of the detector at very low beam currents, where conventional electronics and conventional techniques can be used. By measuring the beam currents at the low and high counting rates, we could estimate to good accuracy the rates at high beam currents. Since unpolarized gun beam is being used for these tests, we arbitrarily assigned + and -'s to the beam pulses using a random number generator. We collected distributions of σ_i^\pm for a sample of beam pulses, for a variety of values of Q. We expect the distributions to have mean values, $\langle \sigma^\pm \rangle$, as shown in Fig. 3, and relative root-mean-square widths, $\Delta\sigma/\langle \sigma \rangle$, which scale as $1/\sqrt{N}$, reflecting the statistical counting fluctuations from pulse to pulse. We plot $\Delta\sigma/\langle \sigma \rangle$ versus $1/\sqrt{Q}$ in Fig. 4. The data points, shown as triangles, can be compared with the solid line, which is the expected values based on the calibration of the counting rate at low beam currents. Figure 4 shows that the fluctuations from pulse to pulse in the flux counting are in good agreement with statistical counting fluctuations. At the highest currents (lowest point in Fig. 4) the pulse to pulse fluctuations are approximately 0.03, corresponding to a counting rate greater than 1000 detected electrons per pulse.

We performed a series of runs from one to three hours in length. For these runs we formed an experimental asymmetry

$$A_{\text{exp}} = \frac{\langle \sigma^+ \rangle - \langle \sigma^- \rangle}{\langle \sigma^+ \rangle + \langle \sigma^- \rangle} \quad (4)$$

using the means of the distributions $\langle \sigma^\pm \rangle$. The error on A_{exp} was calculated from the errors on the means

$$\Delta \langle \sigma^\pm \rangle = \Delta \sigma^\pm (\text{rms width}) / \sqrt{n^\pm} \quad (5)$$

where the number of beam pulses, n^\pm , was for these runs quite large. Figure 5 shows the values of $A_{\text{exp}} / \langle P_e \rangle$ for a sequence of 26 runs. The asymmetries were scaled by $1 / \langle P_e \rangle$, P_e taken to be 0.4, to compare to later asymmetries taken with polarized beam.

The asymmetry averaged for these 26 runs is $(-2.5 \pm 2.2) \times 10^{-5}$. If we plot for each run the deviation of $A_{\text{exp}} / \langle P_e \rangle$ from zero, divided by the error, we obtain the distribution shown in Fig. 6. The expected shape is a gaussian curve of unit width. The data show a standard deviation of 1.02 ± 0.13 , consistent with the expected shape. This result leads us to believe that the errors are properly calculated, and that the techniques used for flux counting can be applied to measuring asymmetries at the level of 10^{-5} .

III. POLARIZED ELECTRON SOURCE

The polarized electron source is shown schematically in Fig. 7. The principle by which this source operates is photoemission of longitudinally polarized electrons from a gallium arsenide crystal using circularly polarized light.² The possibility that this process could provide intense beams of polarized electrons was first suggested in 1974 by Ed Garwin, of SLAC, and D. Pierce³ and H. C. Siegmann of ETH Zürich. The development of such a source to be an injector for the SLAC linac was undertaken at that time by Ed Garwin, C. Sinclair, R. Miller and me.⁴

The source was driven by a flash lamp pumped dye laser operating near 710 nm wavelength. The flash lamp was pulsed at 120 pulses per second, synchronized to the SLAC linac running at the same rate. Pulses of photoemitted electrons, approximately 1.5 μ sec in length and up to 300 milliamperes in intensity, were accelerated from the -65 KeV potential to ground and were transported to the SLAC linac by a series of lenses and d.c. magnets. The longitudinal polarization of electrons leaving the GaAs cathode are negligibly depolarized in the transport system. Beam intensities of 1×10^{11} to 4×10^{11} electrons per pulse were accelerated and delivered to the target. Loss of polarization in the linac was likewise negligible, as demonstrated in earlier tests.⁵

Circular polarization of the laser pump light is achieved in optical polarizers consisting of two elements. These are shown in Fig. 7, and again in detail in Fig. 8. Laser light was first polarized linearly in a calcite prism. Circularly polarization was achieved in a Pockels cell, a uniaxial crystal which exhibits a birefringence linear in the applied electric field. It is cylindrical in shape with ring electrodes around

its circumference. A high voltage pulse, either positive or negative, is applied prior to each beam pulse. Reversing the sign of the high voltage reversed the helicity of the photons, which in turn reversed the helicity of the photoemitted electrons. The reversals were done randomly on a pulse to pulse basis to minimize the effects of drifts on the experiment, and randomization avoided changing the helicity synchronously with any possible periodic changes of beam parameters.

The sign of the Pockels cell voltage was sent to the experimental computer prior to each beam pulse. This allowed us to form our basic experimental quantity:

$$A_{\text{exp}} = \frac{\sigma(V+) - \sigma(V-)}{\sigma(V+) + \sigma(V-)} \quad (6)$$

Throughout the experiment the experimental asymmetry, A_{exp} , is measured relative to the Pockels cell voltage.

The calcite prism was mounted in a rotatable holder; the plane of linear polarization could be rotated by 45° or 90° relative to its 0° position. Rotation of the linear polarization by 90° reversed the helicity of the photons. In general rotation by an angle ϕ_p causes the net helicity to vary by $\cos 2\phi_p$. Since the experimental asymmetry, Eq. (6), is measured relative to the Pockels cell voltage, we expect to find the relation

$$A_{\text{exp}} = \frac{\sigma(V+) - \sigma(V-)}{\sigma(V+) + \sigma(V-)} = |P_e| A \cos(2\phi_p) \quad (7)$$

where $|P_e|$ is the measured beam polarization (around 0.40), and A is the physics asymmetry arising from parity violating effects, defined by Eq. (7).

The rotation of the plane of linear polarization provided a technique which could separate parity violating effects related to helicity of the beam from systematic effects which could arise due to perturbations

of other beam parameters when the Pockels cell voltage was reversed. In Section V the asymmetries measured at 0°, 45° and 90° orientations of the calcite prism are discussed.

IV. BEAM MONITORING

A primary objective of the experimental techniques was to eliminate sources of systematic errors to the extent that corrections to the data were unnecessary. To determine the size of the systematic errors, monitoring of beam parameters which could affect measured cross section values was necessary. The parameters measured were average polarization (sign and magnitude), energy, beam current, beam position and angle at the target.

(a) Polarization: Figure 9 shows a perspective view of the target, magnet, and detector used for determining beam polarization.

The process by which polarization was measured was the elastic scattering of polarized beam electrons by polarized target electrons. The target was a thin foil of a highly permeable alloy of iron (Supermendur). An externally applied magnetic field saturated the material, providing a target with a known fraction (7.8%) of the electrons polarized along the beam direction. Elastic scattering of electrons by electrons (Møller scattering) is a simple QED process and the determination of the spin-dependent part is a straight forward first order QED calculation. We measured the asymmetry

$$A_M = \frac{\sigma_p - \sigma_a}{\sigma_p + \sigma_a} \quad (8)$$

where σ_p (σ_a) is the cross section for Møller scattering with the beam electron spin parallel (anti-parallel) to the target electron spin. For relativistic scattering, at 90° in the e-e center-of-mass, we expected a 100% incident polarization to give a value of $A_M = 0.057$. This value is the result of the QED calculation (7/9) multiplied by the average target polarization (0.078) and the alignment at 20° to the beam direction ($\cos 20^\circ$).

Scattered electrons were detected in a proportional wire chamber hodoscope shower detector, constructed of brass and tungsten. The bins were separated by 4 mm, dividing the lab scattering angle horizontally from 3 mrad to 10 mrad into 24 bins. Momentum was dispersed vertically; elastically scattered electrons fall in a nearly vertical stripe which crossed the center of the hodoscope. At the high rates we encountered, single electron counting was not possible. We measured instead the flux of electrons, using ideas described in Section II. The current for each hodoscope wire was integrated and digitized for each beam pulse. We divided by the incident beam charge Q_i to obtain for each bin and for each beam pulse a cross section σ_{ij} (i^{th} beam pulse, j^{th} bin, units arbitrary). We formed the bin-by-bin asymmetry A_j , using all the beam pulses for a run. Figure 10 shows the results of a typical run. The top figure shows the average cross section $[(\sigma_p + \sigma_a)/2]$ for the 24 bin hodoscope. A clear peak in the center is the e-e scattering peak. This peak sits on a background signal which is largest in the lower bins corresponding to small angles of scatter. This background comes primarily from the radiative tail of elastic Coulomb scattering off the iron nucleus. The lower part of Fig. 10 shows the asymmetry for each bin. The peak asymmetry occurs in the middle

bins, and corresponds to a beam polarization of 35% for this run. The asymmetry for the bins below the elastic peak is non-zero because of the radiative tail for e-e scattering contributes counts in this region. Extraction of beam polarization values requires a subtraction of these background signals, and uncertainties in the procedures leads to uncertainties in the measured polarization values, P_e . We have assigned a ± 0.02 uncertainty on P_e which comes from the uncertainty of the background subtraction. This uncertainty contributed the largest part of the systematic error on the parity violation asymmetry, $\pm 5\%$ of A/Q^2 .

(b) Beam position: Figure 11 illustrates the instrumentation of the beam line. The heart of the beam monitoring system was a resonant microwave cavity with a node which was placed on the beam axis.⁶ Beam pulses passing through the node induced no signals in the cavity. Beam pulses displaced from the node would induce signals proportional to the product of the beam current times the displacement. Using phase-sensitive microwave electronics, both the sign and the amplitude of the signals were measured. By normalizing to the beam current, measured independently, the average displacement pulse by pulse was digitized and stored on tape along with other information for each pulse.

Two resonant microwave position monitors were placed 2 meters before the liquid deuterium target, one sensitive to horizontal displacements, the other sensitive to vertical displacements. These devices provided pulse to pulse measurements of beam position, averaged over the pulse, with resolutions better than 10 μm . The pulse to pulse jitter, arising from instabilities in accelerator pulsed components, was typically 50 μm to 150 μm , varying somewhat with conditions from time to time.

(c) Beam angle: The angle of the beam was measured by a second set of two resonant microwave position monitors placed 50 meters upstream of the target. The measured horizontal and vertical displacements at this location, with information from the positions at the target, provided measurements of the angle of the beam. The system had a resolution better than ± 0.3 μ radians, and pulse to pulse jitter of 1 to 3 μ radians was typical.

(d) Beam current: Beam current was monitored in two separate non-intercepting beam toroid monitors.⁷ Beam pulses induce an impulse in secondary turns on the ferrite toroids. The signals, proportional to the change delivered, were digitized each beam pulse and stored along with other parameters. The toroids have an absolute accuracy better than 1%, and provide the standard charge per pulse used to normalize the signals from the flux counting and beam monitoring instruments. The second toroid monitor served as an independent check on the validity of the main toroid.

(e) Energy: Beam energy was measured with a microwave resonant cavity by measuring displacement of the beam at a location in the beam transport system where energy was dispersed. The sensitivity of the system was $\pm 0.01\%$ from pulse to pulse.

A second redundant energy monitoring system was constructed from two microwave cavities whose anti-nodes were placed on the beam axis, one before the beam transport system and one after. The path length for orbits through the transport system increases with increasing energy, leading to a phase difference between the two microwave cavities which depends on energy. We monitored the phase difference, averaged over

each pulse. Calibration of the system was done by introducing a known phase shift into one side of the phase detector. The resolution of this system exceeded 0.01% per pulse, and the results, which served as a check on the first energy monitor, were in good agreement with the other technique.

(f) Microprocessor feedback: In addition to recording the beam parameters for each pulse, these parameters were monitored with a micro-computer system. When errors were detected, indicating that the beam was drifting away from null values, corrections were applied to beam line elements to return the values to zero. Beam position and beam angle were controlled by adjusting small d.c. magnets before the target. Energy was controlled by adjusting the phase of two accelerator klystrons away from the null value of 90° ; forward from 90° the klystrons could add energy; toward 180° , the klystrons subtracted energy.

The important role the beam monitoring played in the experiment was the determination of the equality (or inequality) of beam parameters between + and - helicities. Differences in + and - beam position can lead to measured asymmetries through geometric effects; energy differences could enter through the cross section dependence, and current imbalances could generate systematic asymmetries through electronic non-linearities. Quantitative estimates of the sensitivity to these imbalances were made through several techniques; calculation of geometric effects through Monte Carlo work, and estimation of position angle and energy dependence from known cross section formulae. Sensitivity to current imbalances were measured. These results are summarized in Table I. The parameters quoted are the differences between + and - helicity beams. The first column

summarizes the imbalance which leads to a 1×10^{-5} asymmetry. The second column shows the measured imbalance for the combined data. We treat these results as corrections to the asymmetries, but in addition increase the systematic errors by the same amount. This procedure reflects the preliminary nature of our errors; the understanding of systematic errors should improve with further study of the present and future data.

V. THE DATA

This part will describe the data in some detail. The techniques of flux counting, described in Section I, and polarization reversals, described in Section III, give us the basic experimental asymmetry, A_{exp} , defined by Eq. (6). This experimental quantity, formed in the computer using the rapid random reversals of helicity, is stable even in the presence of drifts in the experimental apparatus. In addition to the rapid polarization reversals using the Pockels cell, two other methods for reversing beam helicity were available to us. They were:

- (1) Rotation of the plane of linear polarization, before the Pockels cell, by rotating the calcite prism in its mount.
- (2) Precession of the electron spin relative to its direction, due to the electron anomalous magnetic moment ("g-2 precession"), by taking data at different beam energies.

These two methods serve as consistency checks on our procedures; the experimental asymmetries should follow the expected changes if sources of systematic errors are negligible. In particular, each method contains null points where asymmetries are expected to vanish, and any non-zero

measurements can arise only from systematic effects. Thus the measurements can place limits on systematic errors, independent of the results obtained from beam monitoring data.

We take data with the calcite prism set at three discrete orientations:

- (a) Prism at 0° , producing + (-) helicity electrons for + (-) Pockels cell voltage;
- (b) Prism at 45° , producing unpolarized electrons for either sign of Pockels cell voltage; and
- (c) Prism at 90° , producing - (+) helicity electrons for + (-) Pockels cell voltage.

We expect to see the $\cos(2\phi_p)$ dependence for the experimental asymmetry of Eq. (7).

Figure 12 shows the results at 19.4 GeV for $A_{\text{exp}}/|P_e|$ obtained in the shower counter. For the 45° point, we used a value 0.37 for $|P_e|$. In addition, the results of the unpolarized gun beam data described in Section II, are shown, using the same value for $|P_e|$. The dashed curve is the expected $\cos(2\phi_p)$ form, fit to the 0° and 90° points. The 0° and 90° asymmetries are equal and opposite within errors, and the 45° point is consistent with zero, as expected. The errors shown are statistical only. No systematic corrections have been applied to these data.

Figure 13 shows in detail the thirteen runs which constitute the 45° data point. There are two questions of interest; first, what is the average value of these asymmetries, and second have we assigned the errors properly? The average value, $(1.0 \pm 3.0) \times 10^{-5}$, is shown in Fig. 12. The second question is answered by looking at the deviation from zero

relative to the assigned errors. Figure 14 shows the standard deviation about the mean. The solid curve is a gaussian of unit width. The thirteen runs exhibit a standard deviation of 0.67 ± 0.13 .

The sequence of 44 runs which resulted in the 0° and 90° points of Fig. 12 is shown in Fig. 15. The prism was rotated from 0° to 90° and then back every few runs. The 0° runs are shown as solid points; the 90° runs as open points. The runs are typically 1 to 3 hours in length. By changing the sign of the asymmetries measured with the prism oriented at 90° , we can ask the same two questions as above. The average value of the asymmetries is $(-14.9 \pm 1.5) \times 10^{-5}$, and the distribution about this mean is shown in Fig. 16. The standard deviation of the 44 runs is 1.00 ± 0.11 , consistent with the expected gaussian curve of unit width. This distribution shows that the errors assigned are correct, and furthermore, that the asymmetries observed are distributed throughout our data, rather than being associated with a few spurious runs.

These results, summarized by Fig. 12, contain two null measurements, which are satisfied within statistical accuracy, and two consistency checks which are satisfactory. The null measurements are the zero asymmetries obtained with unpolarized electrons from the SLAC gun and from the (unpolarized) GaAs source, and the consistency checks are the two data points at 0° and 90° , which are equal and opposite, and the standard deviations of the data in Figs. 14 and 16, which are consistent with the expected normal distribution.

These data described in Figs. 12 and 16 were obtained from the shower counter. An additional check on the validity of the data is seen in Fig. 17, where results for the gas Cerenkov counter are shown. The

asymmetries are independently determined from flux counting measurements made on this counter. This counter is not statistically independent, since the same electrons detected in this counter pass through and are counted in the shower counter, but this counter has independent electronics, and responds quite differently to possible sources of backgrounds. Thus, we conclude that the measured asymmetries do not arise from an artifact of electronics or from unknown background counts of some kind.

Reversals of beam helicity can be achieved by the g-2 precession of the polarized electrons. At 19.4 GeV the helicity of the beam at the target was positive for positive Pockels cell voltage. However, the helicity depended on beam energy, owing to the anomalous magnetic moment of the electron, and the 24.5° deflection of the beam passing through the transport magnets. The spin precesses relative to the beam direction by

$$\theta_{\text{prec}} = \frac{E_0}{m_e} \left(\frac{g-2}{2} \right) \theta_{\text{bend}} = \frac{E_0 (\text{GeV})}{3.237} \pi \text{ radians} \quad (9)$$

where m_e is the mass and g is the gyromagnetic ratio of the electron.

For the experimental asymmetry we expect

$$A_{\text{exp}} = |P_e| A_{\text{phys}} \cos \left[\frac{E_0 (\text{GeV})}{3.237} \pi \right] \quad (10)$$

Table II gives the kinematic parameters for the data taken at four beam energies. The asymmetries $A_{\text{exp}}/|P_e|Q^2$ are shown in Fig. 18 for the shower counter and Fig. 19 for the Cerenkov counter. In these figures we plot $A_{\text{exp}}/|P_e|Q^2$ because at different beam energies, the average Q^2 for the scattering varies. We expect A to grow linearly in Q^2 ,⁸ and the quantity plotted to show the $\cos \frac{E_0 \pi}{3.237}$ dependence. The point at $E_0 = 17.8$ GeV provides a third null test for this experiment. At this energy,

electrons are transversely polarized as they pass through the target, and asymmetries from highly relativistic transversely polarized electrons are expected to vanish. The orientation of the spectrometer is such that the transverse polarization is normal to the scattering plane of the electrons for $E_0 = 17.8$ GeV. The data point measured here, consistent with zero asymmetry, gives experimental evidence that the measured asymmetries do not arise from transverse components of the spin.

Figures 18 and 19 constitute the ultimate experimental evidence that the observed asymmetries are associated with electron spin. No systematic effects or influence the source may have on the beam parameters can mimic the $g-2$ precession which arise from the anomalous magnetic moment of the electron and beam transport geometry.

Based on the results shown in Figs. 12, 17, 18 and 19, we conclude that parity violation exists in this process. To determine the magnitude, we exclude the lowest energy point, because it contains fairly strong elastic and resonance contributions and is the lowest Q^2 point, where the nucleon model, used for deep inelastic scattering, is least likely to apply. The data point at 19.4 GeV and 22.2 GeV (with its sign changed) are combined to give

$$A/Q^2 = (-9.5 \pm 1.6) \times 10^{-5} (\text{GeV}/c)^2 (\text{deuterium}). \quad (11)$$

The sign implies negative helicity electrons have a greater probability for scattering than do positive helicity electrons. The quoted error is derived from a statistical error of $\pm 0.86 \times 10^{-5}$ added linearly to estimated systematic uncertainties of 5% in the value of $|P_e|$ and of 3.3% from asymmetries in beam parameters. The π^- background contributed less

than 0.1×10^{-5} to A/Q^2 , but normalization corrections of 2% for π^- background and 3% for radiative corrections were made.

VI. IMPLICATIONS FOR GAUGE THEORIES

The high degree of interest in parity violation in the weak neutral currents arises from the ability of such effects to discriminate between different gauge theory models. The experimental observation of existence of neutral current processes, originally reported in 1973 by the Gargamelle collaboration at CERN,⁹ has to be considered a major success for the general ideas of gauge theories which proposed to unify the weak and electromagnetic interactions into one force of nature. Experimental information on the detailed nature of neutral currents was meager in the following several years. In the absence of experimental information, a number of models were proposed. Parity non-conservation in the neutral currents is a central issue because experimentally measurable effects arise that can be related to neutral current coupling constants. Neutrino cross section measurements are in principle unable to distinguish between parity violating models and more complex gauge theories which preserve parity invariance in the underlying dynamics while explaining the neutrino-anti-neutrino cross section difference as a consequence of comparing left handed neutrinos with right handed anti-neutrinos. This is seen in a class of gauge theory models (the left-right symmetric models) where the neutral currents are explained by the exchange of two or more neutral heavy bosons. In the case of neutrino scattering the single photon exchange is absent.

The couplings are vector-vector for one and axial vector-axial vector for the other; the relative signs change from neutrino to anti-neutrino, but parity is conserved. These models predict no parity violation for electromagnetic processes, such as the one reported here. The popularity of these models has been enhanced, of course, by the reported absence of parity violation in atomic bismuth.^{10,11} The results of this experiment appear to contradict the atomic bismuth results and almost certainly exclude those left-right symmetric models which have parity conserved. The issue of parity violation in atoms is unresolved, and is being actively pursued at present.

The simplest gauge theories are those based on the $SU(2) \times U(1)$ gauge group. The original form, the Weinberg-Salam (W-S) model of the weak interactions, has the left handed electron and quarks assigned to weak isospin doublets, while the right handed quarks and electrons are singlets. Prediction of parity violation in inelastic scattering of electrons (and muons) can be made, but requires the knowledge of the hadronic vertex. Predictions have been made by a number of authors.¹²⁻¹⁷ The usual assumption is to treat the nucleon in the simple quark-parton model.¹⁸ The scattering is taken as an incoherent process off 3 valence quarks only (for deuterium, six quarks). The neutral current couplings are specified in this model by the mixing parameter, $\sin^2 \theta_W$, where θ_W is the Weinberg angle, and by the weak isospin assignment for the u,d quarks and for the electrons. The predicted asymmetries have the form

$$A/Q^2 \cong -10^{-4} f(\sin^2 \theta_W, y) \quad (12)$$

$$\cong a g_A^e G_V^q + b h(y) g_V^e G_A^q \quad (13)$$

where $y = \nu/E_0$ is the fractional energy transfer to the hadrons, and $h(y) \equiv (1 - (1-y)^2)/(1 + (1-y)^2)$. The asymmetries arise from vector-axial vector cross products between electrons and hadron coupling constants. The hadron terms come from sums over quark constituents. Following the arguments of Cahn and Gilman, if we take the left handed weak isospin assignments as determined to be doublets, and take all possible right handed combinations (either doublets or singlets) there are 8 possible $SU(2) \times U(1)$ "models" or predicted asymmetries. These are shown in Fig. 21, as a function of $\sin^2\theta_W$, for $y = 0.21$, the only value for which we have data. The measured asymmetry is shown on the right margin, and the cross-hatched region corresponds to the upper and lower extremes of the error bars. Three of the models, those with the electron in a doublet along with one or both quarks assigned to right handed doublets, are immediately excluded. Two more models, $(b^u)_R$ and $(b^u)_R (d^t)_R$, can be also excluded because they require large values of $\sin^2\theta_W$, inconsistent with neutrino data. A sixth model, $(b^u)_R$ is in a good agreement with our data, but fails a more detailed study of neutrino results.¹⁹ Only two models remain of the original eight. One of these has the electron assigned to a doublet, $(E_e^0)_R$, while the other is the original Weinberg-Salam model. Figure 22 shows these two models in detail. The y -dependence is shown for the W-S model (solid lines) and for the "mixed" or "hybrid" model (dashed lines) for values of $\sin^2\theta_W$ shown. The measured asymmetry has inner error bars which are statistical only, and outer errors which are obtained by adding the systematic errors linearly. The agreement with the W-S model is satisfactory, provided

$$\sin^2\theta_W = 0.20 \pm 0.03 \quad (14)$$

while agreement with the hybrid model is questionable, requiring a value of $\sin^2 \theta_W < 0$. The hybrid model gives a predicted asymmetry which is 3 standard deviations from the measured value if $\sin^2 \theta \approx 1/4$.

Near the end of the available running time, we took a limited amount of data at 19.4 GeV using a liquid hydrogen target. The result was

$$A/Q^2 = (-9.7 \pm 2.7) \times 10^{-5} (\text{GeV}/c)^{-2} (\text{hydrogen}). \quad (15)$$

This result is shown in Fig. 23, again with the W-S and hybrid models also shown. The proton target is treated as two u and one d quark compared to the equal mix for deuterium, and asymmetries are expected to be slightly smaller. Our result is consistent within errors with this expectation and with the result obtained from deuterium.

REFERENCES

1. S. Stein, et al., Phys. Rev. D12, 1884 (1975).
2. D. T. Pierce, et al., Phys. Lett. 51A, 465 (1975), and Appl. Phys. Lett. 26 (1975).
3. E. L. Garwin, D. T. Pierce and H. C. Siegmann, Swiss Physical Society Meeting, April 26, 1974; Helv. Phys. Acta 47, 393 (1974) (abstract only). The full paper is available as SLAC-PUB-1576 (1975) (unpublished).
4. C. K. Sinclair, et al., in High Energy Physics with Polarized Beams and Targets, proceedings of the Argonne Symposium, edited by M. L. Marshak (AIP, New York, 1976), p. 424.
5. P. S. Cooper, et al., Phys. Rev. Lett. 34, 1589 (1975). This experiment used the same target as Ref. 5, but used a different spectrometer and detectors.
6. Z. D. Farkas, et al., SLAC-PUB-1823, 1976 (unpublished).
7. R. S. Larsen and D. Horelick in Proc. of Symposium on Beam Intensity Measurement, DNPL/R1, Davesburg Nuclear Physics Laboratory, April 1968 and SLAC-PUB-398 (1968).
8. This fact arises from the electromagnetic amplitude, which has a $1/Q^2$ dependence, giving an asymmetry proportional to Q^2 .
9. F. J. Hassert, et al., Phys. Lett. 46B, 191 (1973) and F. J. Hasert et al., Phys. Lett. 46B, 138 (1973).
10. L. L. Lewis, et al., Phys. Rev. Lett. 39, 795 (1977), and
11. P. E. Baird, et al., Phys. Rev. Lett. 39, 798 (1977).
12. A. Love, et al., Nucl. Phys. B49, 513 (1972).
13. E. Derman, Phys. Rev. D7, 2755 (1973).
14. W. W. Wilson, Phys. Ref. D10, 218 (1974).
15. S. M. Berman and J. R. Primack, Phys. Rev. D9, 2171 (1974) and Phys. Ref. D10, 3895 (1974) (erratum).

16. M.A.B. Beg and G. Feinberg, Phys. Rev. Lett. 33, 606 (1974).
17. S. M. Bilenkii, et al., Sov. J. Nucl. Phys. 21, 657 (1975).
18. R. N. Cahn and F. J. Gilman, Phys. Rev. D17, 1313 (1978).
19. L. F. Abbott and R. M. Barnett, Phys. Rev. Lett. 40, 1303 (1978).

TABLE I
SYSTEMATIC ERRORS SUMMARIZED

(a) Beam Monitoring - Deuterium target runs

<u>Parameter</u>	<u>Units</u>	<u>Measured Difference</u>		<u>Correction to A/Q^2</u>
		(+)	(-)	
E_0	0/0	$(1.5 \pm .28) \times 10^{-4}$		$-.37 \times 10^{-5}$
Q	ma	$(-2.2 \pm .4) \times 10^{-3}$		-.03
X_T	μm	$(-8.9 \pm 3.3) \times 10^{-2}$		+0.04
Y_T	μm	$(-.65 \pm 1.8) \times 10^{-2}$		-.02
θ_x	μrad	$(-.37 \pm .7) \times 10^{-3}$.00
θ_y	μrad	$(1.5 \pm .9) \times 10^{-3}$		<u>+0.01</u>
				$-.37 \times 10^{-5}$

(b) Beam Monitoring - Hydrogen target runs

E_0	0/0	$(-2.4 \pm .44) \times 10^{-4}$		$+0.50 \times 10^{-5}$
Q	ma	$(1.9 \pm 1.3) \times 10^{-3}$		+0.4
X_T	μm	$(12.7 \pm 2.5) \times 10^{-2}$		-.05
Y_T	μm	$(2.8 \pm 1.8) \times 10^{-2}$		-.02
θ_x	μrad	$(-1.5 \pm .59) \times 10^{-3}$.00
θ_y	μrad	$(-3.0 \pm .75) \times 10^{-3}$		<u>+0.03</u>
				$+0.50 \times 10^{-5}$

(c) Polarization determination - $\pm 5\%$ of A/Q^2 added to error.

TABLE II

Beam Energy	g-2 Precession Angle	Spectrometer Setting	Kinematic Quantities Averaged Over Spectrometer	
E_0 (GeV)	θ_{prec} (rad)	E' (GeV)	Q^2 (GeV/c) ²	y
16.18	5.0 π	12.5	1.05	.18
17.80	5.5 π	13.5	1.25	.19
19.42	6.0 π	14.5	1.46	.21
22.20	6.9 π	17.0	1.91	.21

FIGURE CAPTIONS

1. A schematic overview of the experiment. The two-mile accelerator (LINAC) is fed electrons from either the unpolarized SLAC gun or polarized electrons from the gallium arsenide source. Beam monitoring of position, angle, current, energy and polarization measure systematic errors. Detection of electrons scattered by a 30 cm liquid deuterium target is done in a spectrometer instrumented with a gas Cerenkov counter and a lead glass shower counter.
2. Acceptance of electrons is shown superimposed on experimental cross section values, measured in earlier work (Ref 1). Negative π cross section is also shown.
3. Linearity test of gas Cerenkov counter operating in flux counting mode. Cross section, measured in arbitrary units, is independent of beam current delivered to target.
4. Relative width for cross section values taken from measured distributions using flux counting techniques, is $1/\sqrt{Q}$, where Q is the charge per pulse delivered to the target. The points lie on the solid line, obtained by calibration at very low beam currents, where single particle counting works well. The agreement shows that flux counting exhibits the statistical fluctuations expected.
5. Measured asymmetries, $A_{\text{exp}}/|P_e|$, for 26 runs using the unpolarized gun beam.
6. Standard deviations about zero for the 26 runs using the unpolarized gun beam. The solid curve is the expected shape, a normal curve of unit width.

7. A schematic view of the gallium arsenide polarized electron source. Polarized electrons are photoemitted from the GaAs crystal using circularly polarized laser light. Electrons accelerate from -65 KV potential, are deflected out of the laser beam and transported to the injector.
8. A detailed view of the laser polarizing optics. A calcite prism first linearly polarizes the light. A Pockels cell circularly polarizes the light to $\pm 100\%$ for $\pm V$ applied to its ring electrodes. The experimental asymmetries are formed from beam pulses of + and - V. Rotation of the calcite prism through an angle ϕ_p about the axis of the beam should modulate the experimental asymmetry by $\cos 2\phi_p$.
9. The Møller spectrometer, target, and detector shown in a perspective view. Forward scattered electrons are deflected in the magnetic field while beam particles pass through the center of a septum and are undeflected. A proportional wire chamber hodoscope of 24 bins detects scattered electrons.
10. Typical Møller cross section and asymmetries for the 24 bins. Increasing bin number corresponds to increasing lab angle. The elastic e-e peak stands in the center above a background. The size of asymmetry observed corresponds to $P_e \approx 35 \pm 2\%$ for this run. Measurements were made at full beam intensity.

11. A schematic layout of beam monitoring equipment. Microwave resonant cavities placed on the beam line form the position sensors for the system. Horizontal and vertical position and angle are monitored at the end of the accelerator and before the target. Current toroids monitor charge delivered to the target. Energy monitors were obtained from two systems: a position monitor at the center of the transport line, and a phase detector attached to cavities before and after the beam transport system. A minicomputer detected error signals and feedback corrections to beam line magnets and to accelerator klystrons to stabilize position, angle, and energy.
12. Experimental asymmetries, divided by $|P_e|$, for the lead glass shower counter, for the three prism orientations 0° , 45° , and 90° . The dotted line is the expected $\cos 2\phi_p$ curve, normalized to 0° and 90° . The asymmetry measured with the unpolarized gun beam is also shown.
13. Experimental asymmetries, divided by $|P_e|$, for 13 runs taken at a prism orientation of 45° .
14. Standard deviations about mean for 13 runs with prism at 45° .
15. Experimental asymmetries, divided by $|P_e|$, for 44 runs taken at 0° and 90° prism orientation.
16. Standard deviations about mean for 44 runs taken at 0° and 90° prism orientation. The signs of asymmetries at 90° have been changed.
17. Experimental asymmetries, divided by $|P_e|$, for the gas Cerenkov counter, for the three prism orientations. These data should be compared with the data for the lead glass shower counter, Figure 12.

18. Experimental asymmetries, divided by $|P_e|Q^2$, for lead glass shower counter, at four beam energies. The dotted curve shows the modulation of the asymmetry expected from the g-2 precession of the electron spin in the $24\frac{1}{2}^\circ$ bend of the beam transport.
19. Experimental asymmetries, divided by $|P_e|Q^2$, for the gas Cerenkov counter, at the four beam energies. The results for this counter should be compared to those for the shower counter, Figure 18.
20. $SU(2) \times U(1)$ gauge theory model predictions for $\sin^2\theta_W$, for a deuterium target at $y = 0.21$. The experimental result is shown on the right hand margin. The cross hatched area covers the experimental limits. Eight $SU(2) \times U(1)$ models are labelled by the right handed doublets as in Ref. 17.
21. The y-dependence for the deuterium target asymmetry A/Q^2 for two $SU(2) \times U(1)$ models and for values of $\sin^2\theta_W$ shown. The two models considered are the standard Weinberg-Salam model (solid curves) and the hybrid model which assigns the right handed electron to a doublet with an hypothesized heavy neutral lepton (dashed curves). Our data point is shown at $y = 0.21$ with inner error bars (statistical only) and outer error bars (systematic errors added to statistical errors).
22. The y-dependence for hydrogen target asymmetries for the same case described in Figure 21. The model predictions differ slightly because of the different mix of quarks. The data point has larger errors than the deuterium case because of lower counting rates (fewer target nucleons) and shorter running time for this point.

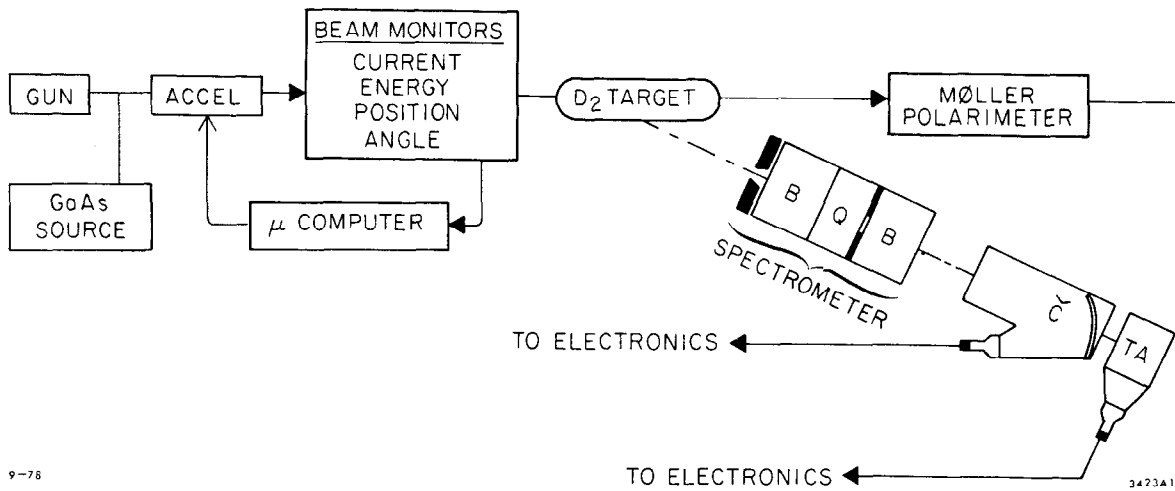
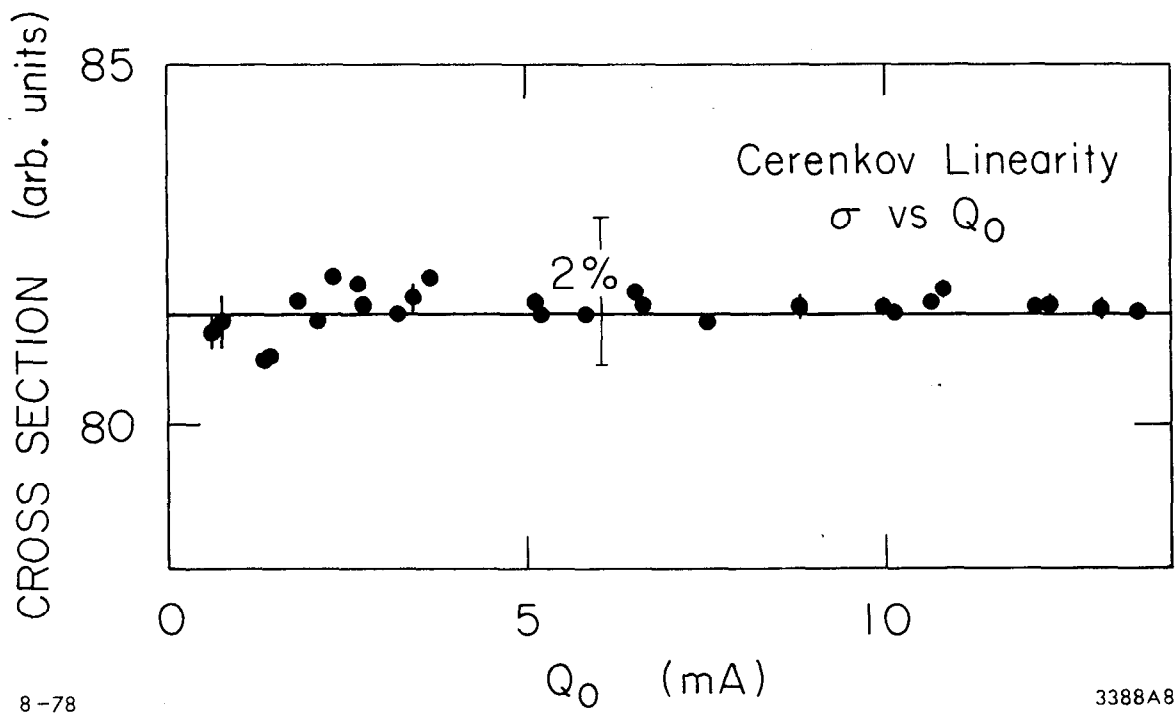


Fig. 1



8-78

3388A8

Fig. 3

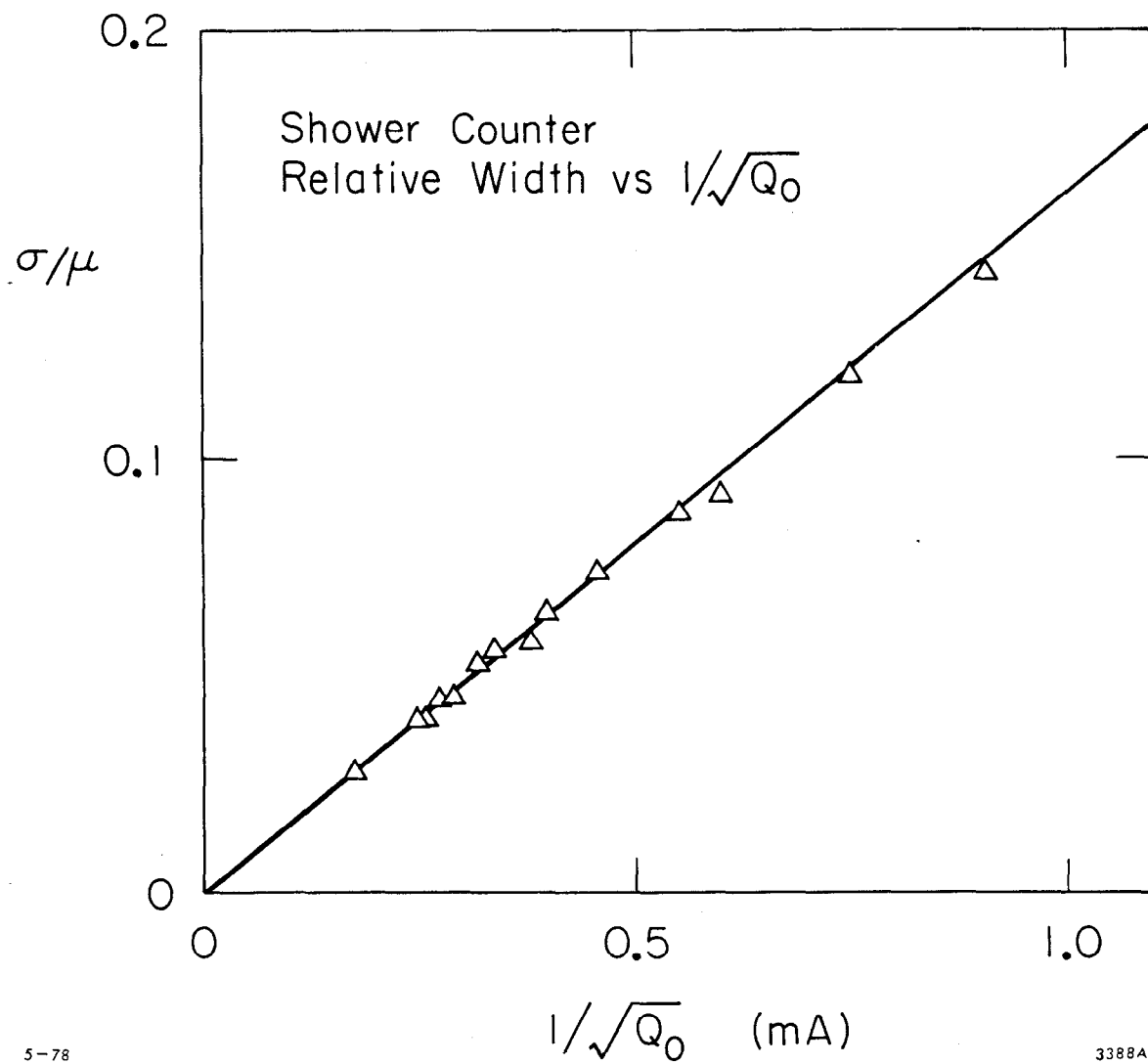


Fig. 4

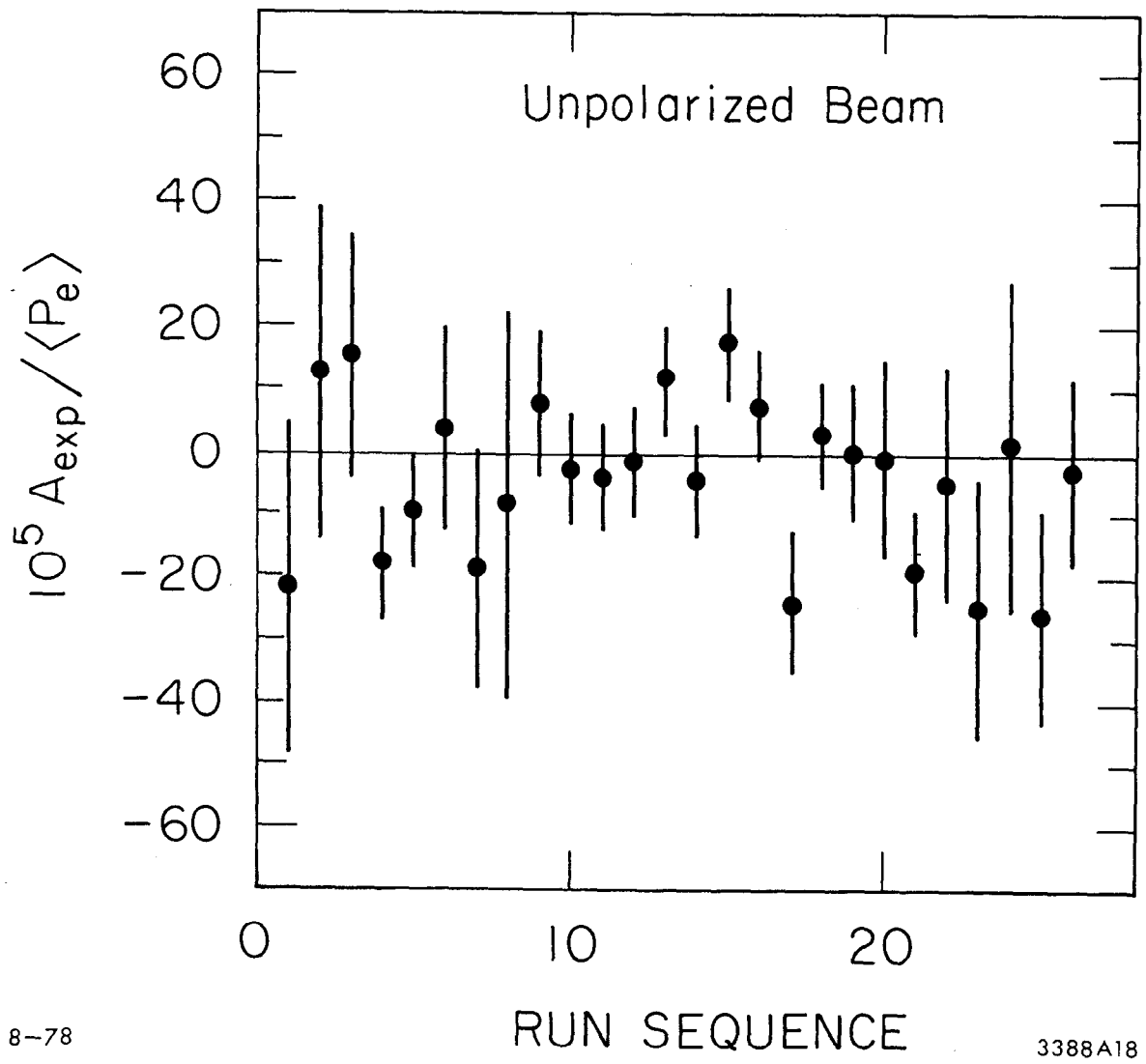


Fig. 5

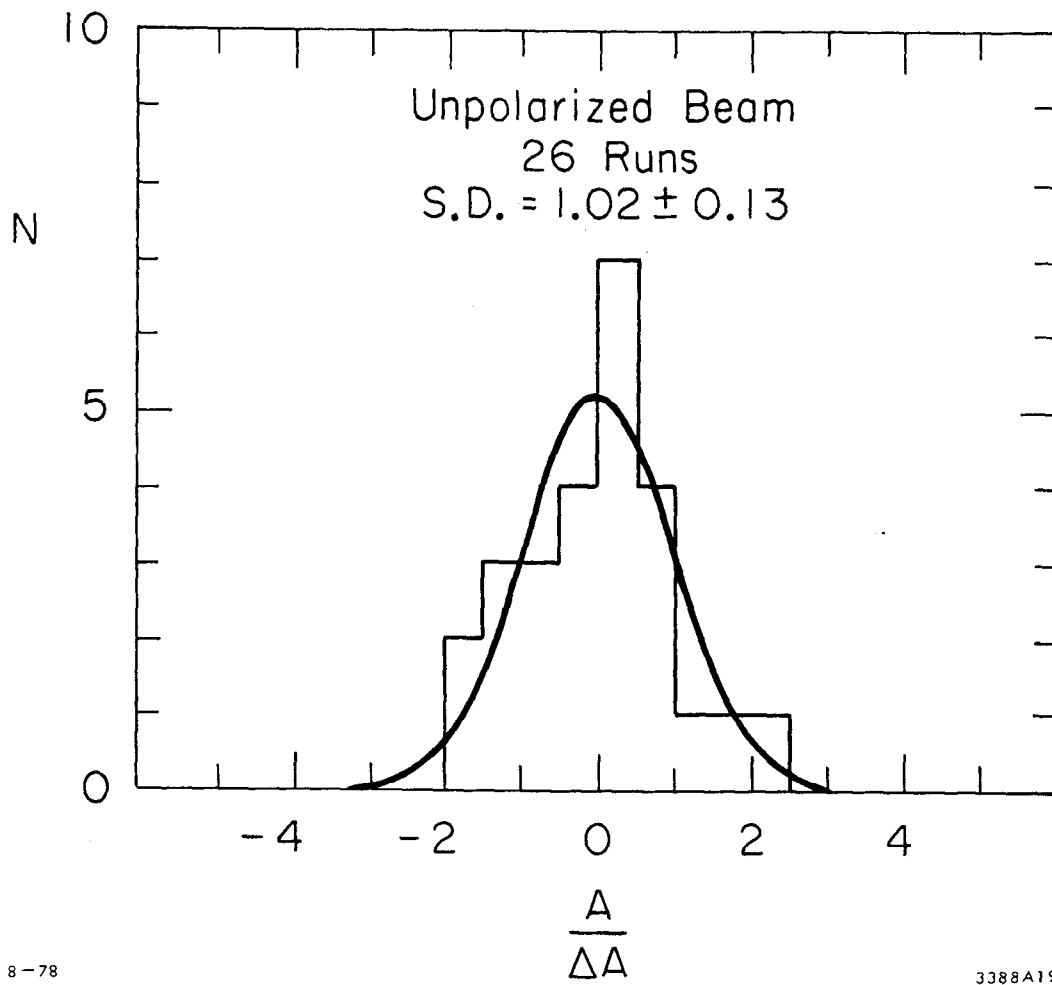


Fig. 6

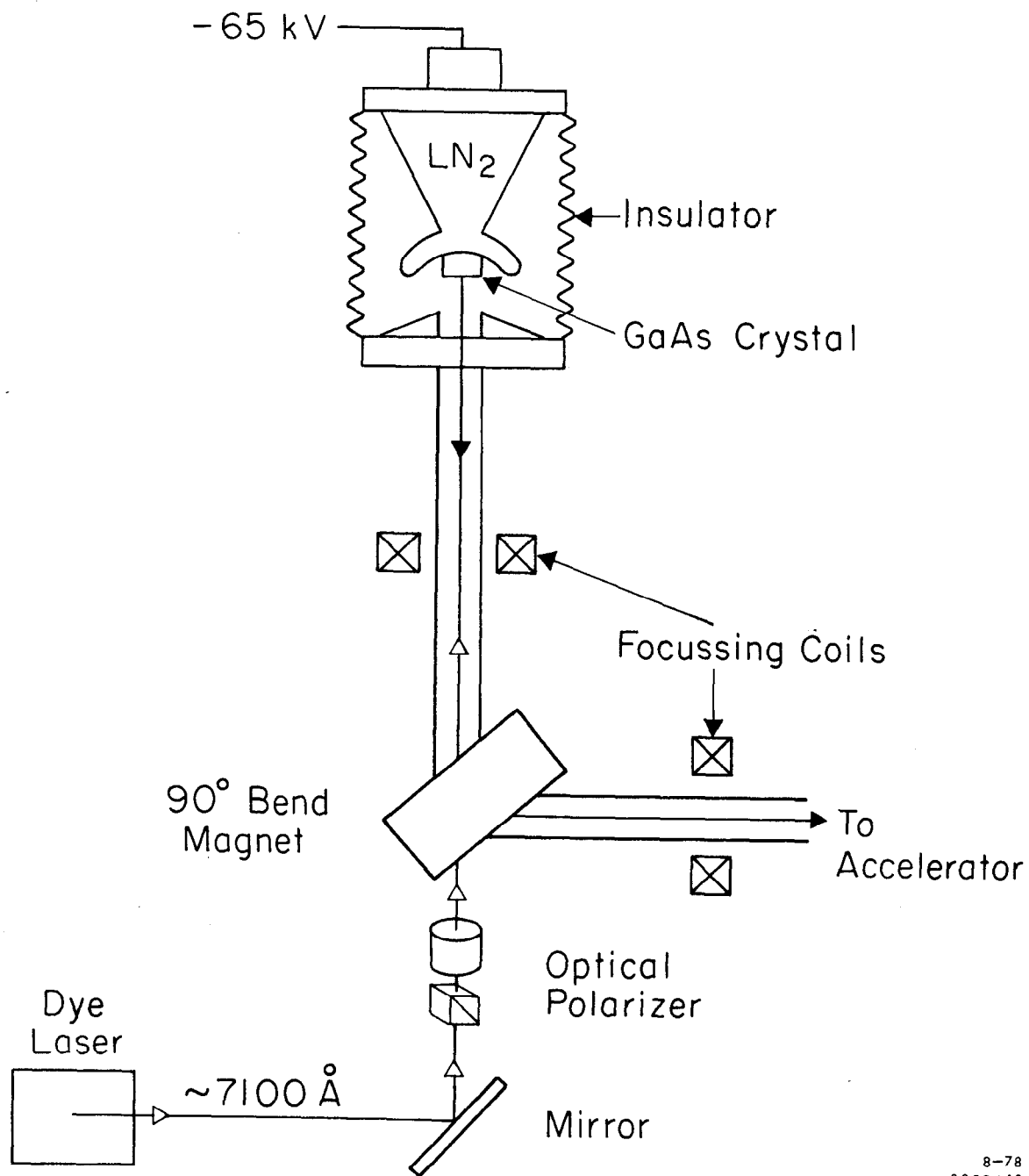
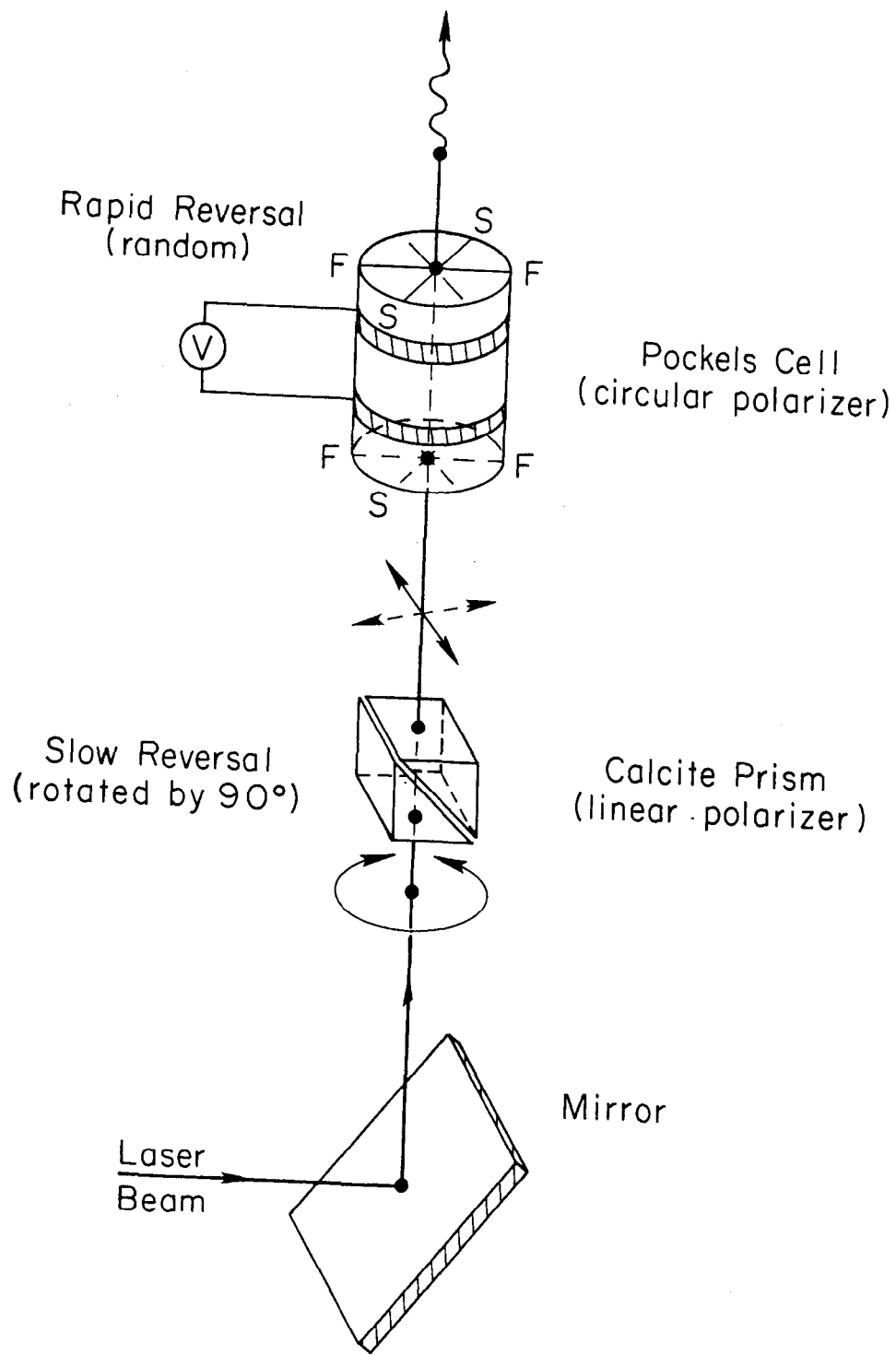


Fig. 7



4-78

OPTICAL REVERSAL SCHEME

3388A3

Fig. 8

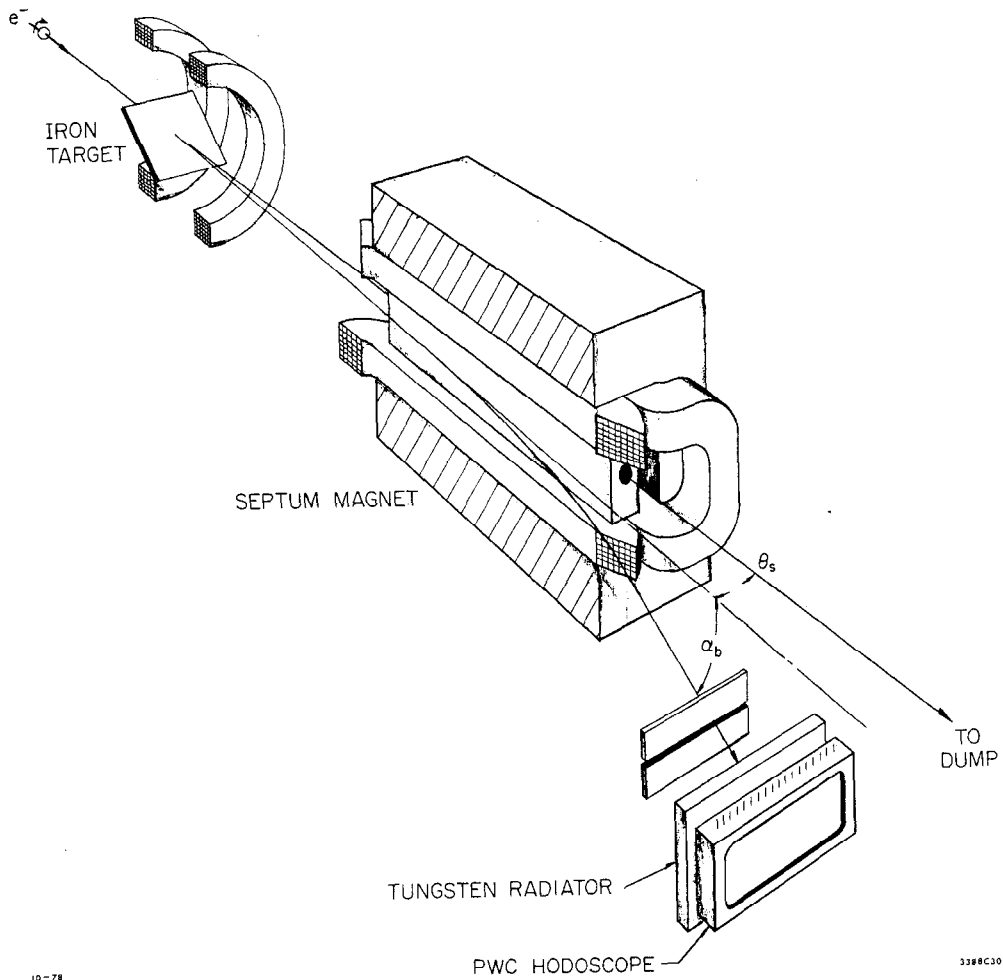
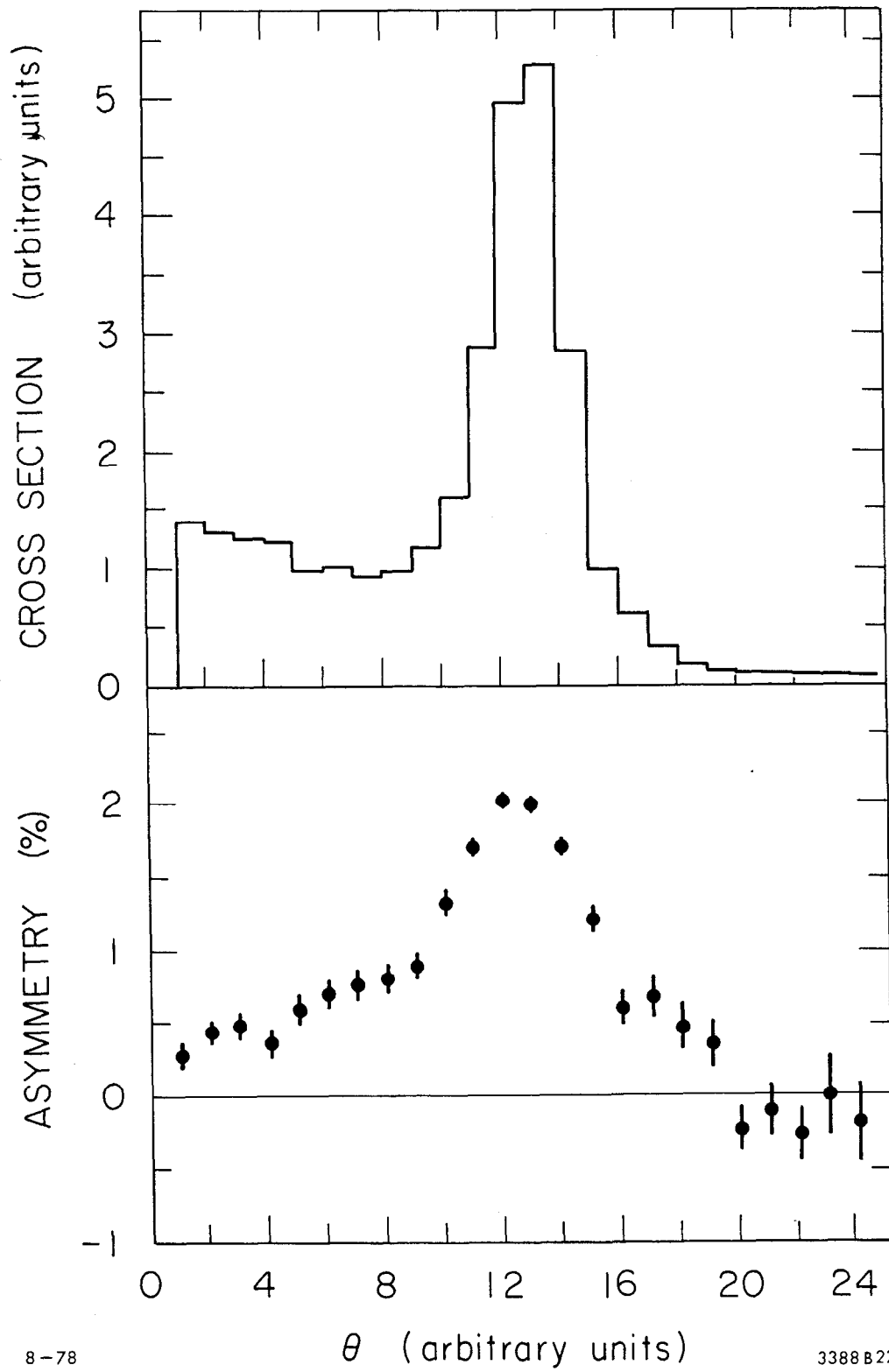


Fig. 9



8-78

3388B22

Fig. 10

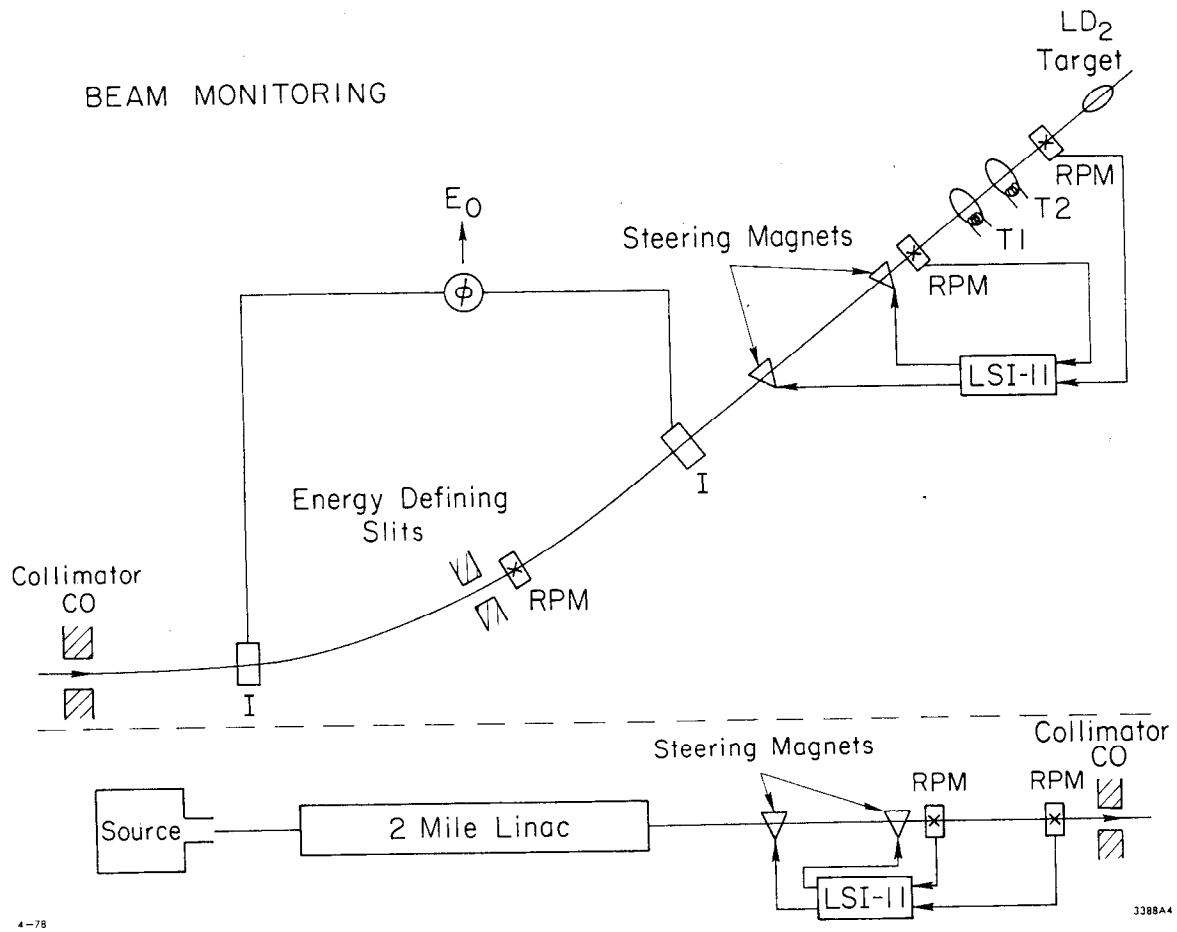


Fig. 11

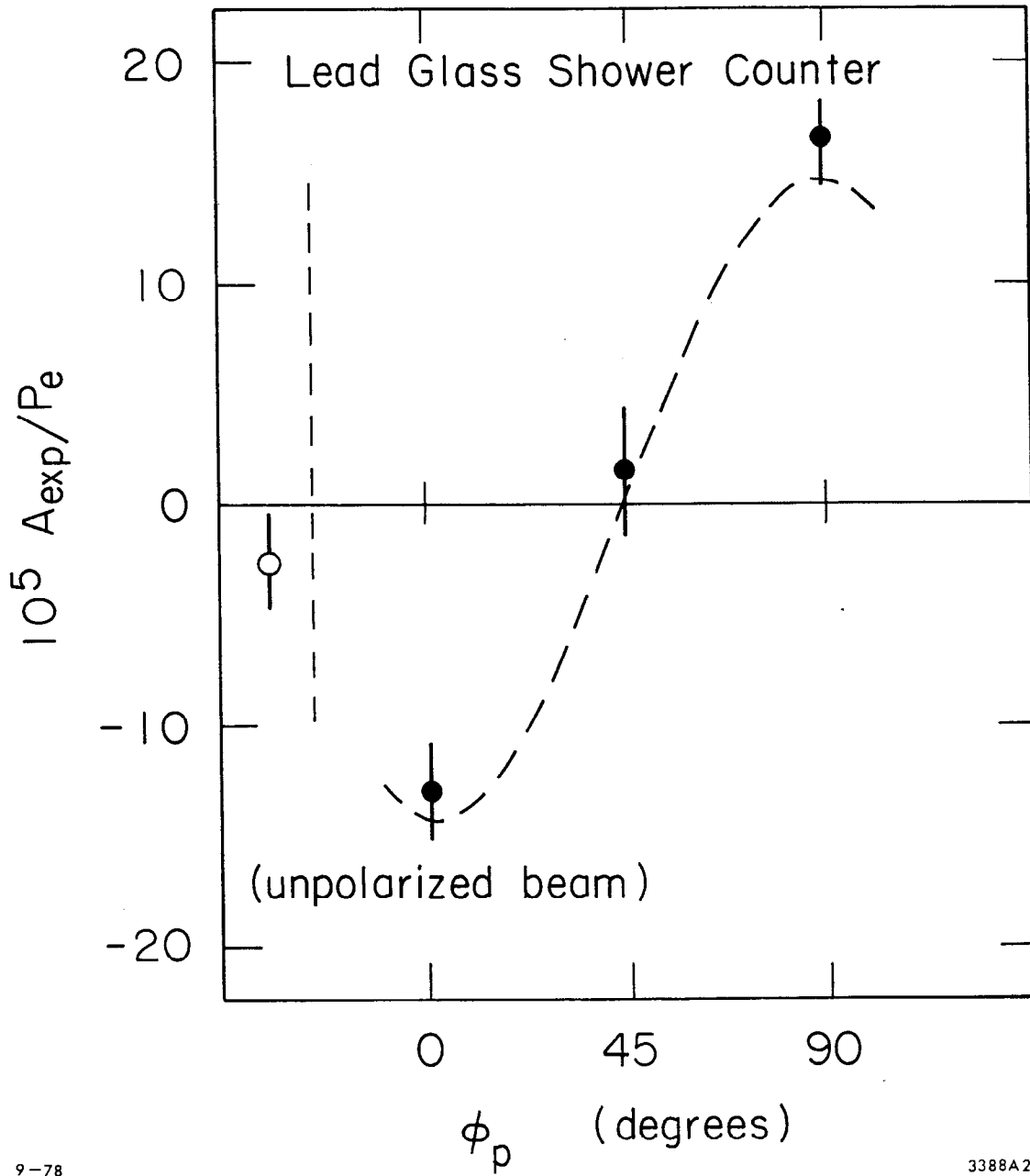


Fig. 12

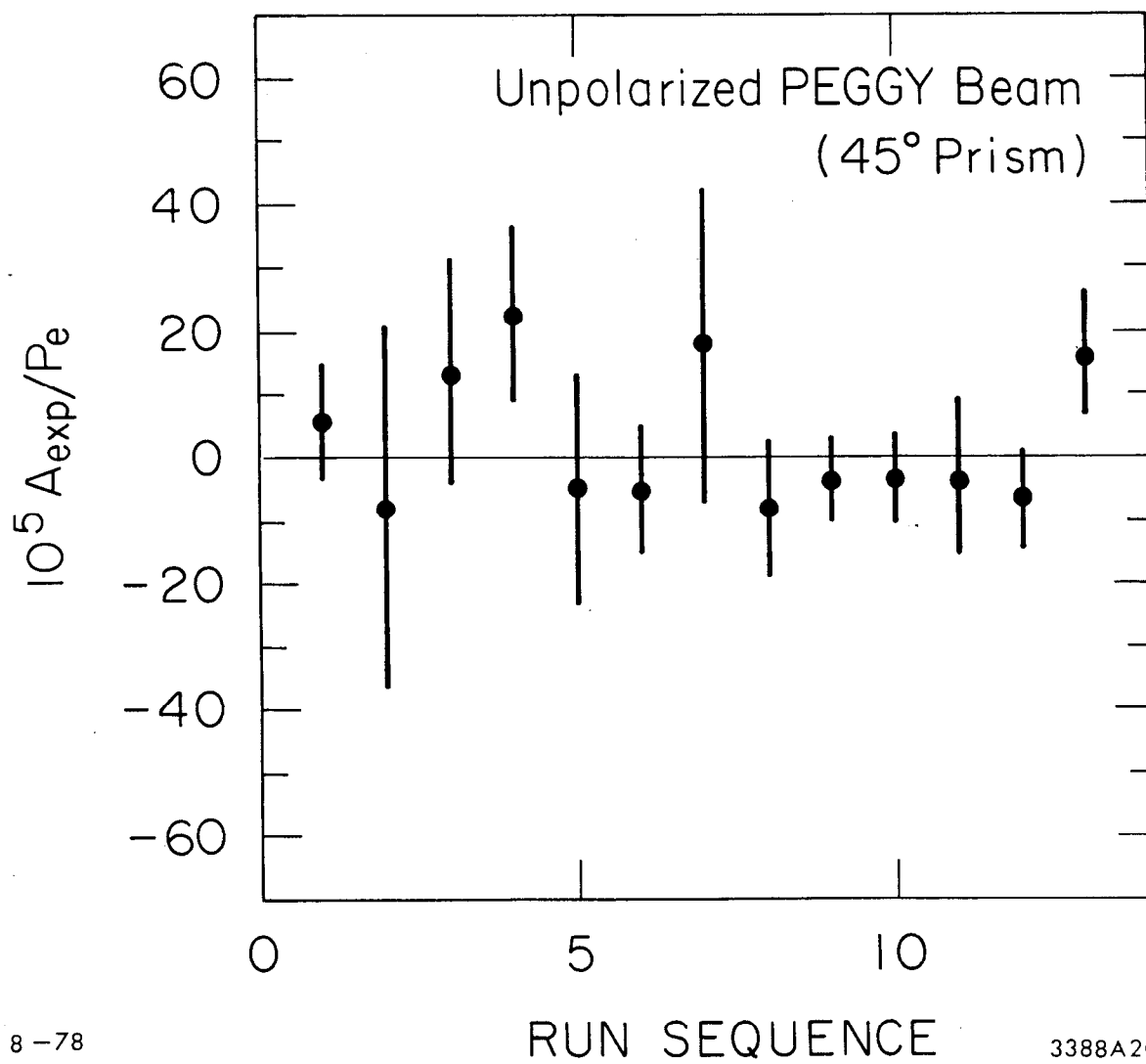


Fig. 13

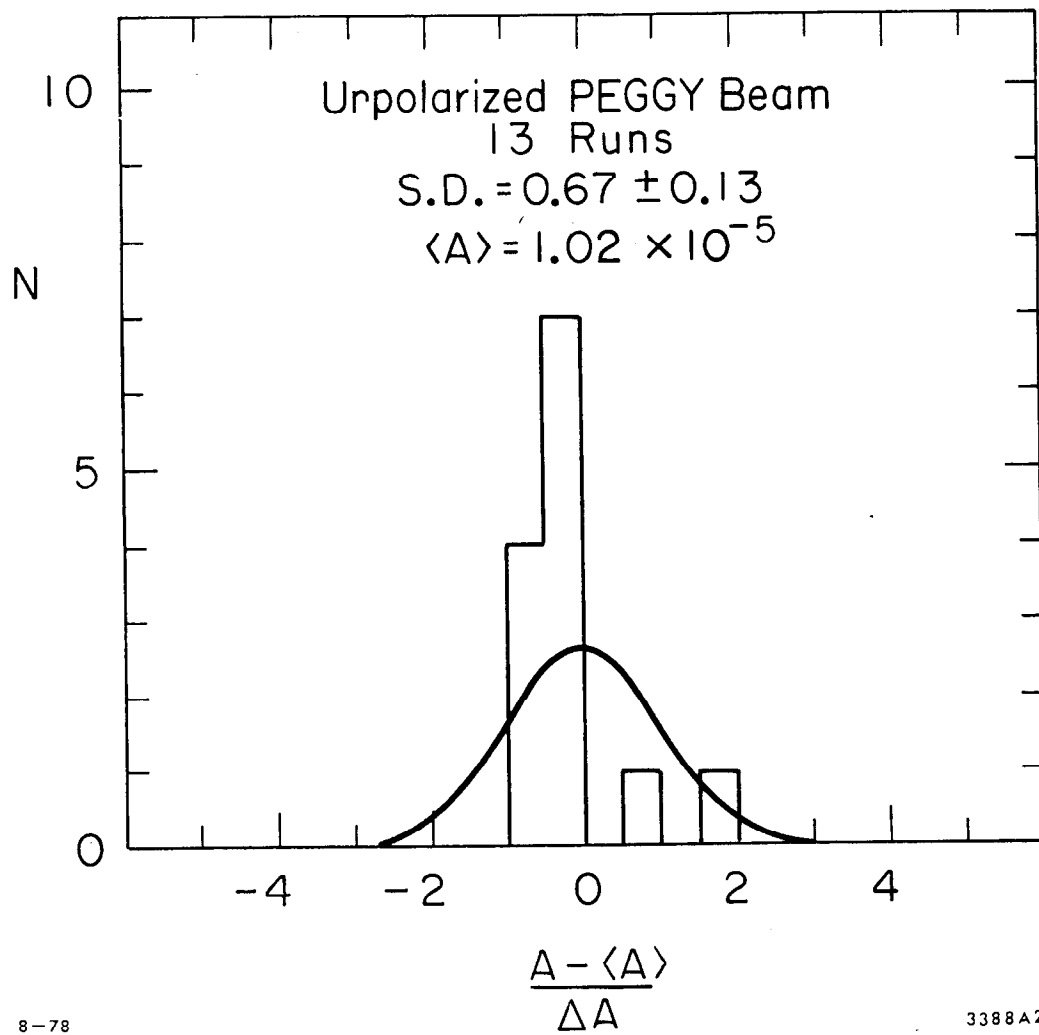


Fig. 14

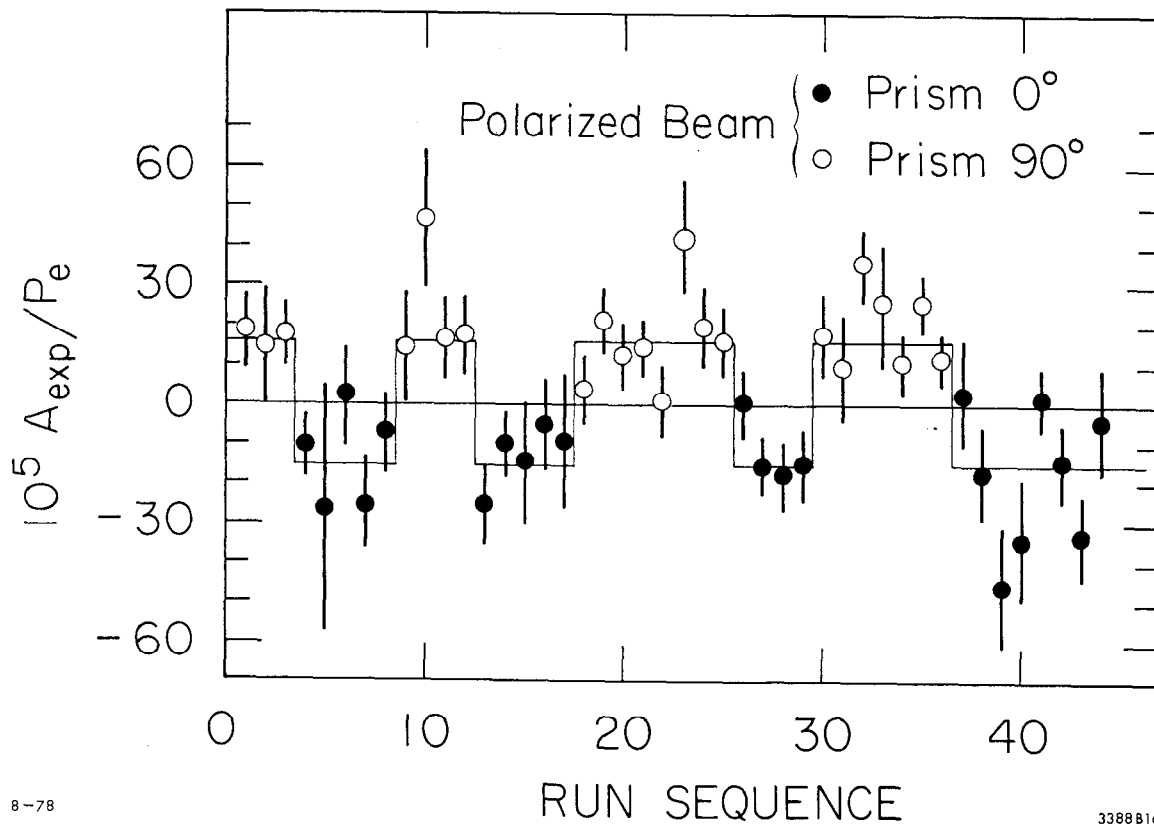


Fig. 15

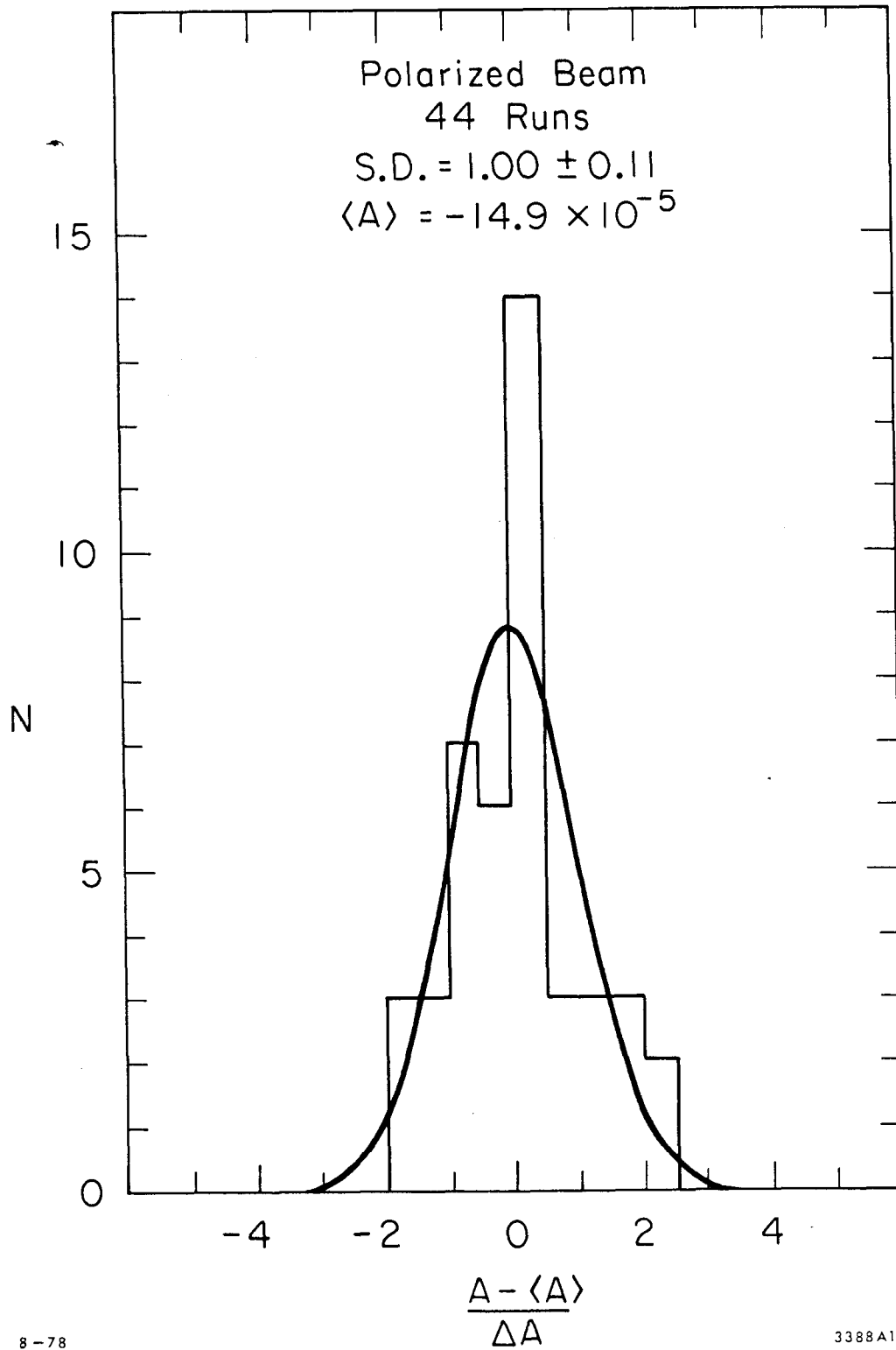


Fig. 16

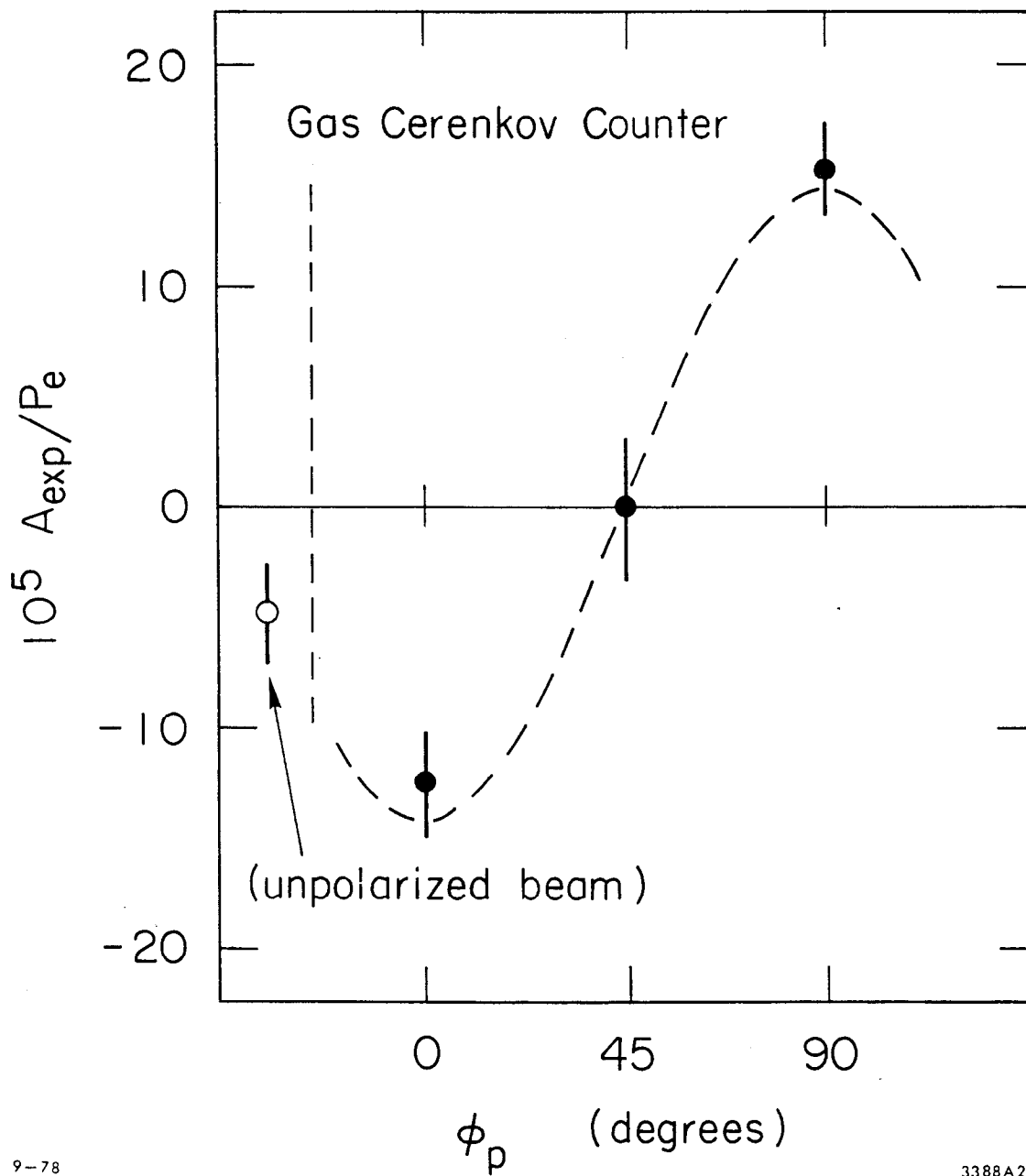


Fig. 17

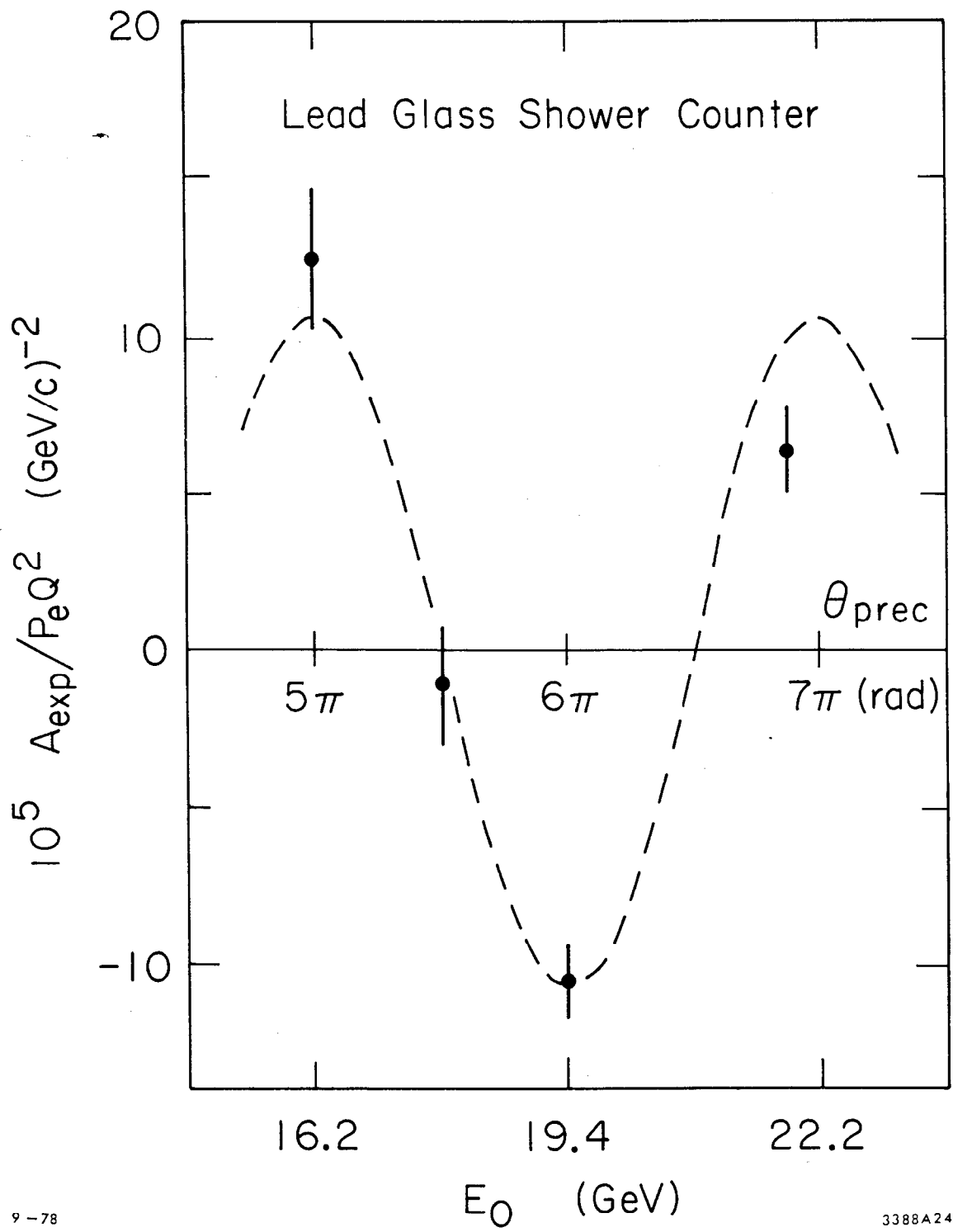


Fig. 18

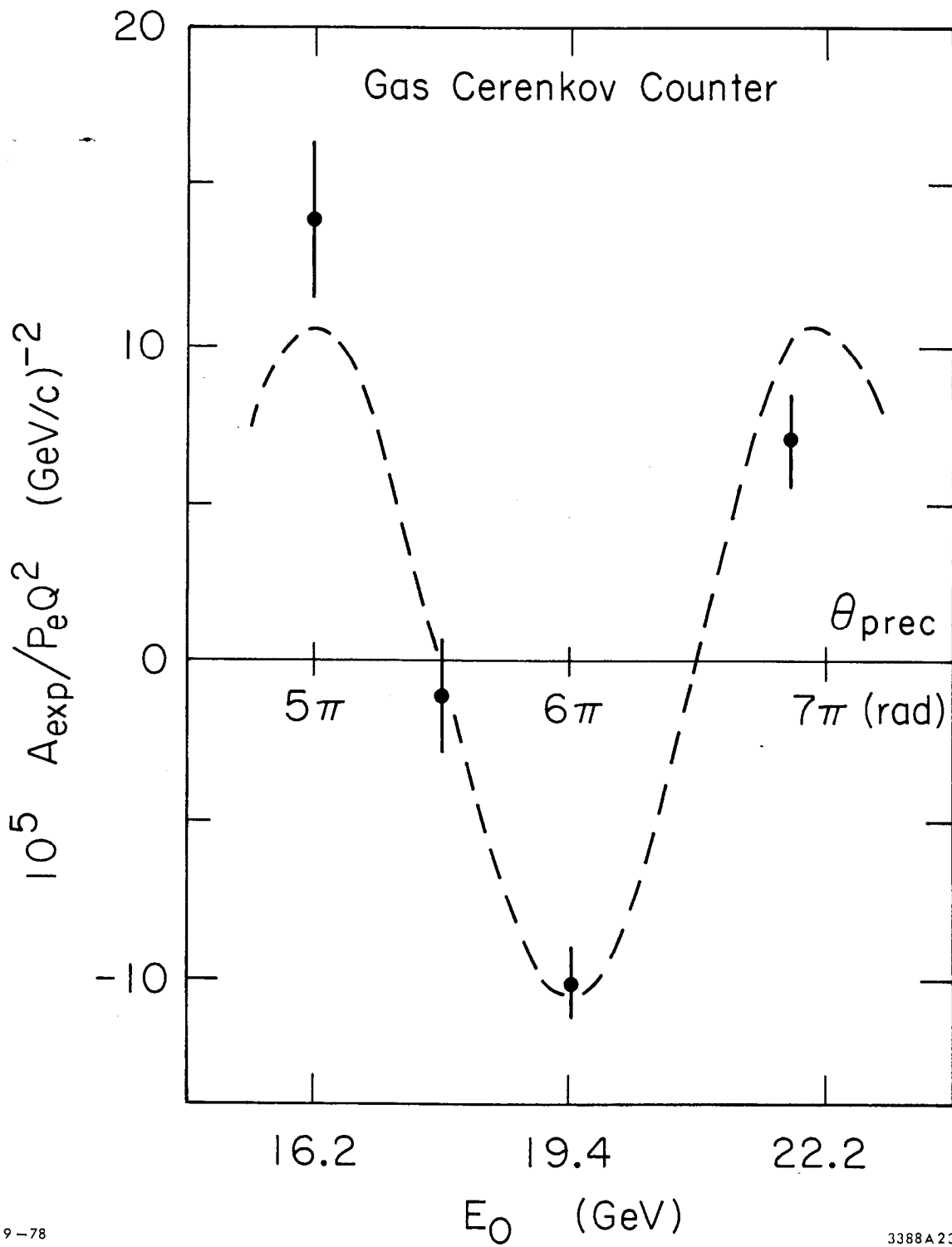


Fig. 19

DEUTERIUM TARGET
 $y = 0.21$

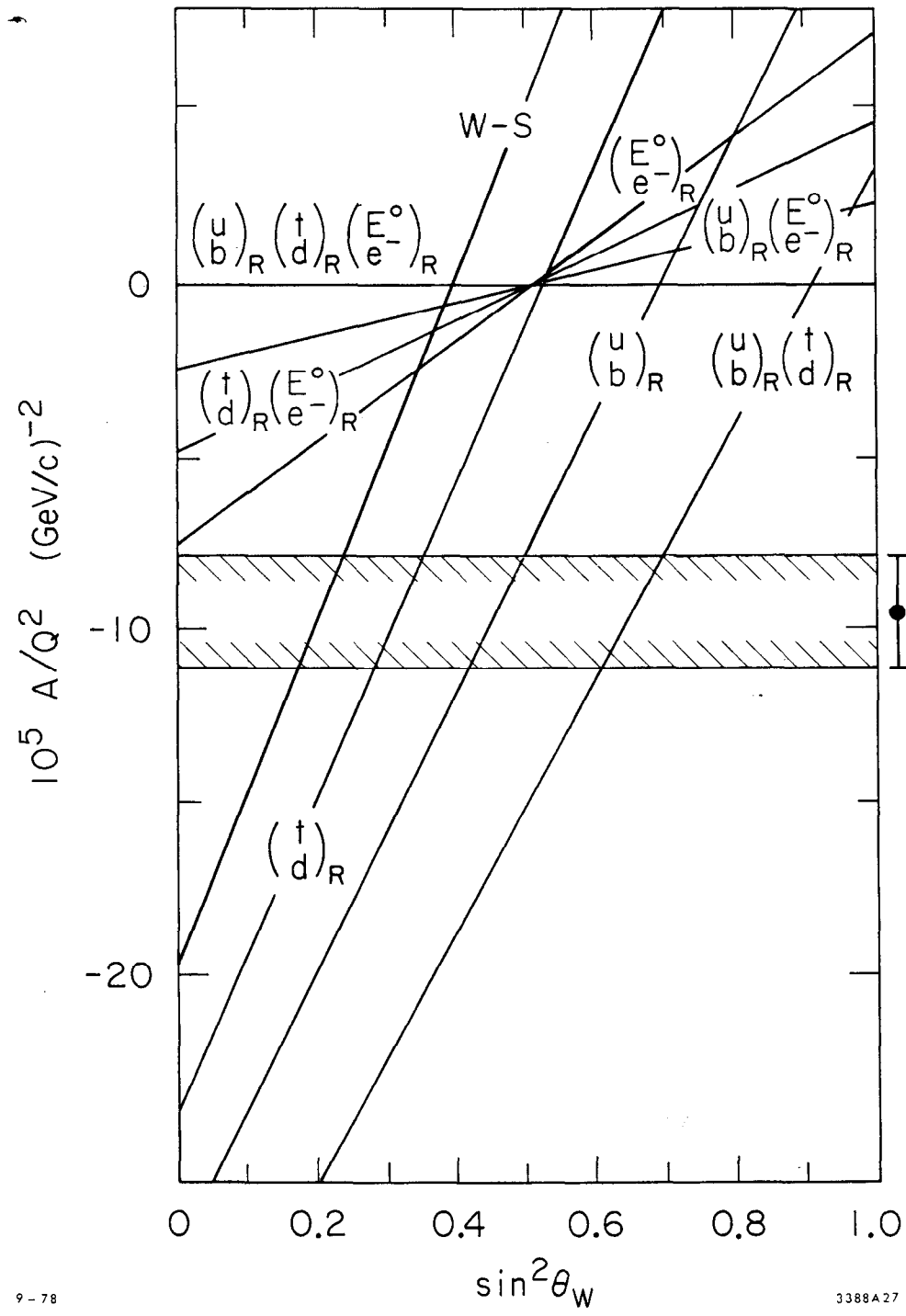
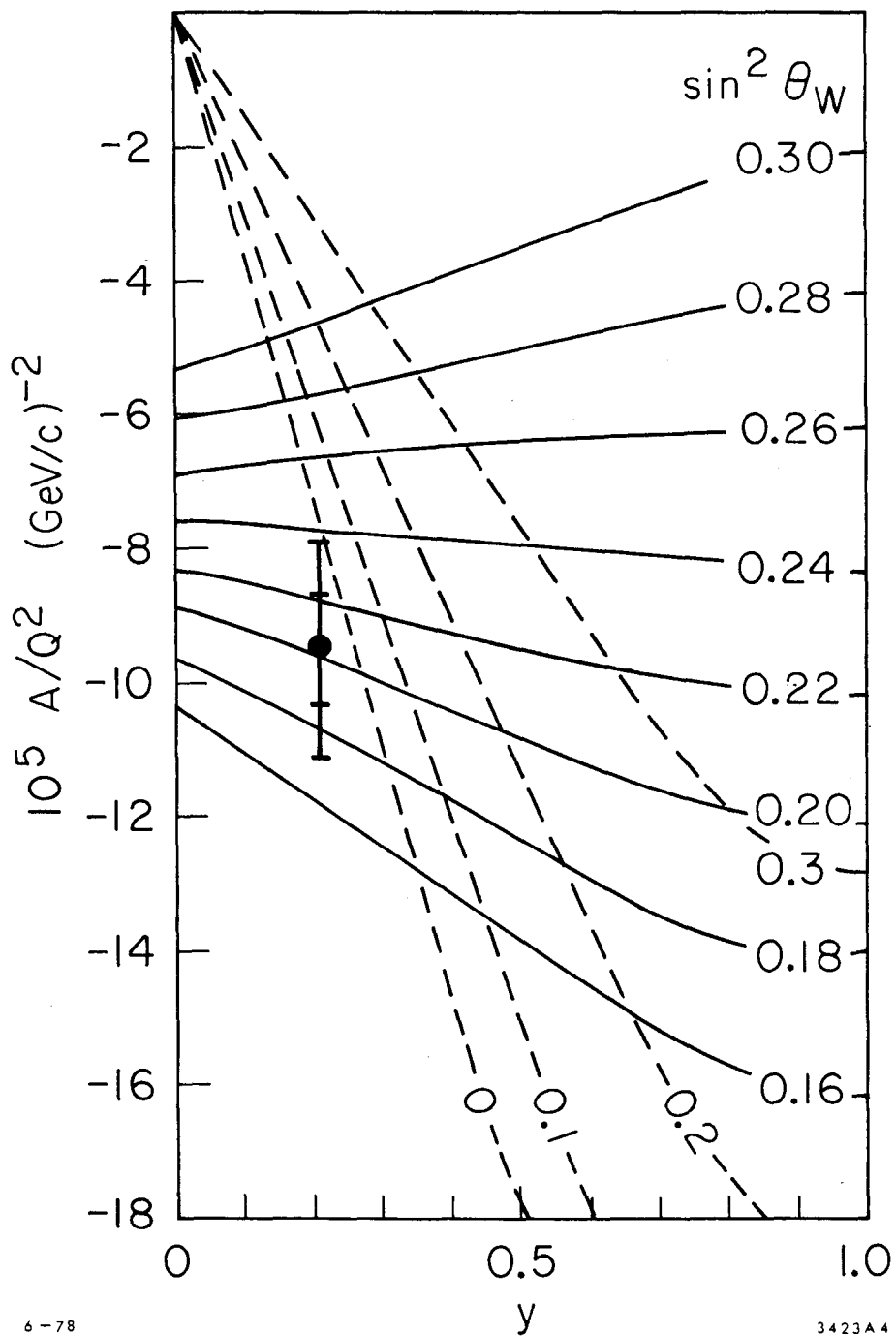


Fig. 20

DEUTERIUM TARGET

— W-S - - - $\left(\frac{E^0}{e^-}\right)_R$



6-78

3423A4

Fig. 21

HYDROGEN TARGET

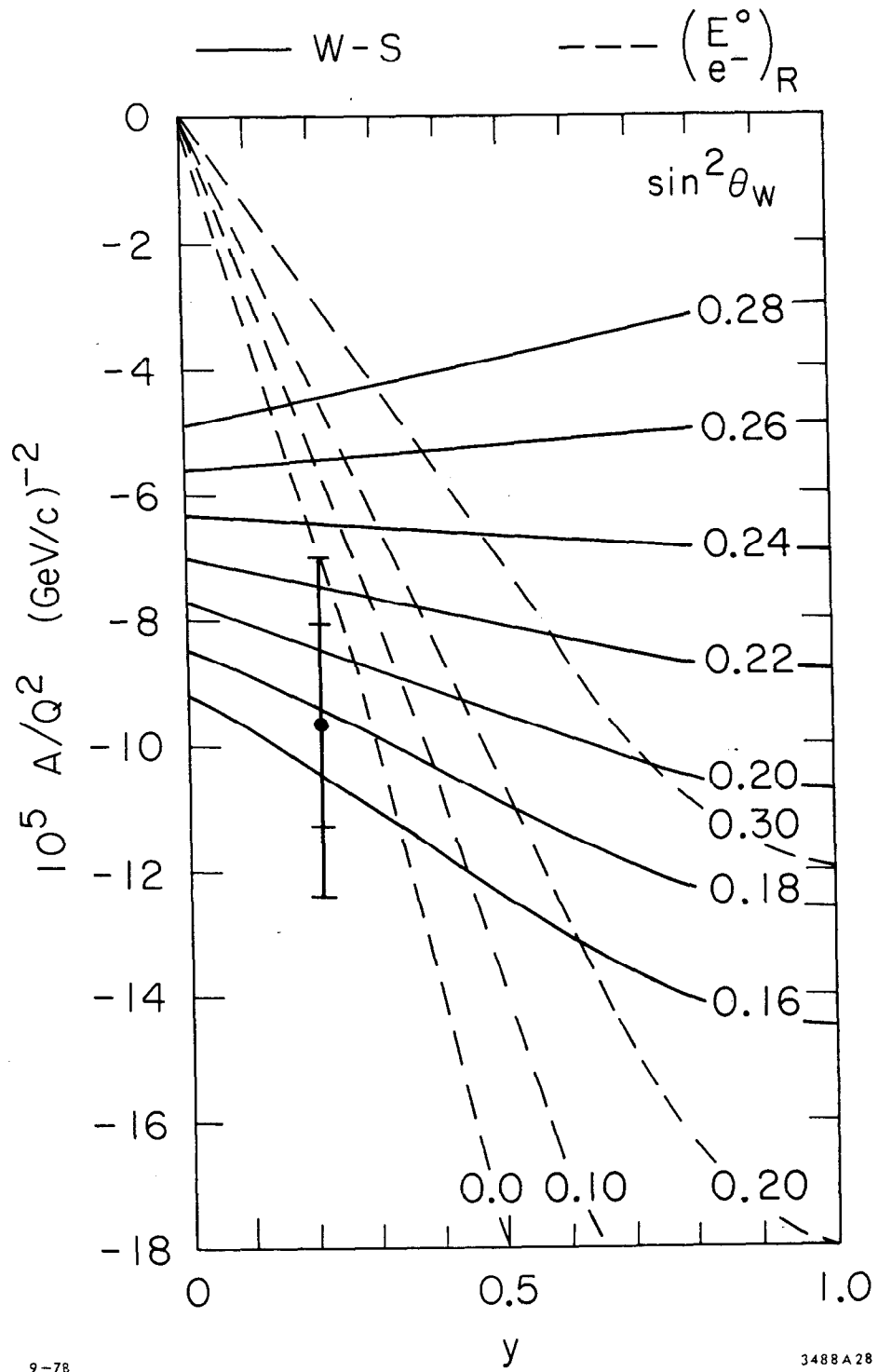


Fig. 22